

Relativistic and wide-angle corrections to galaxy power spectra

Sheean Jolicoeur^{1,a}, Sêcloka L. Guedezounme^{2,b},
Roy Maartens^{2,3,4}, Pritha Paul⁵, Chris Clarkson^{5,2},
Stefano Camera^{6,7,8,2}

¹Department of Physics, Stellenbosch University, Matieland 7602, South Africa

²Department of Physics & Astronomy, University of Western Cape, Cape Town 7535, South Africa

³Institute of Cosmology & Gravitation, University of Portsmouth, Portsmouth PO1 3FX, UK

⁴National Institute for Theoretical & Computational Sciences, Cape Town 7535, South Africa

⁵School of Physics & Astronomy, Queen Mary University of London, London E1 4NS, UK

⁶Dipartimento di Fisica, Università degli Studi di Torino, Torino, 10125, Italy

⁷Istituto Nazionale di Fisica Nucleare, Sezione di Torino, Torino, 10125, Italy

⁸Istituto Nazionale di Astrofisica, Osservatorio Astrofisico di Torino, Pino Torinese, 10025, Italy

E-mail: ajolicoeursheean@gmail.com, seclokaguedezounme@gmail.com

Abstract. Galaxy surveys contain information on the largest scales via wide-angle and relativistic contributions. By combining two different galaxy populations, we can suppress the strong cosmic variance on ultra-large scales and thus enhance the detectability of the signals. The relativistic Doppler and Sachs-Wolfe effects are of a similar magnitude to the leading wide-angle corrections, so that it is important to treat them together, especially since they can partially cancel. The power spectra depend on the choice of line of sight for each galaxy pair and we present results for a general line of sight. Then we estimate the detection significance of the auto- and cross-power spectra for a variety of cases. We use two futuristic galaxy samples based on a ‘beyond-DESI’ survey and a SKA Phase 2 survey, covering $15,000 \text{ deg}^2$ up to $z = 1$. We find a detection significance for the total relativistic wide-angle effects that ranges from $\sim 5\sigma$ to $> 15\sigma$, depending on the line-of-sight configuration.

Contents

1	Introduction	1
2	Relativistic and wide-angle corrections in the number counts	2
3	Auto- and cross-power spectra	5
4	Illustrating the relativistic and wide-angle effects	8
5	Detecting the relativistic and wide-angle effects	9
6	Conclusions	15
A	Fourier kernels	17
B	Coefficients $C_{lmn}^{(ab)}$	18
C	Multipoles of the power spectra	20

1 Introduction

The dark matter density contrast can be traced by galaxies, allowing us to probe the Universe and thus test cosmological models and gravity itself. The underlying dark matter distribution imparts peculiar velocities to galaxies, which distort the galaxy positions along the line of sight. These redshift-space distortions are dominated by the Kaiser effect but also include further relativistic effects [1–4]. In a Fourier space analysis of redshift-space distortions, it is common to use the plane-parallel or flat-sky approximation in which the line-of-sight direction from an observer to different galaxy pairs is fixed.

For next-generation surveys with wide sky coverage, the flat-sky limit cannot be expected to deliver the necessary theoretical accuracy. In fact it is necessary for consistency to include the relativistic corrections with the wide-angle corrections – since they are of the same order of magnitude on ultra-large scales. Furthermore, these corrections can reinforce each other and can also partially cancel each other, depending on the properties of the tracers. A theoretically complete solution requires a full-sky analysis, using the 2-point correlation function or its angular harmonic (or spherical Fourier-Bessel) transform and including all wide-angle and relativistic contributions [3–8].¹ However this is computationally very intensive and a simpler approach is the approximate inclusion of leading-order wide-angle corrections to the plane-parallel limit (see e.g. [15–17]). Recent works have included relativistic effects in the wide-angle corrections of the galaxy power spectrum [18] and its multipoles [19–23].

In this paper, we follow the perturbative approach adopted by [22]. We generalise their result from the midpoint line of sight to all possible lines of sight. We include the standard redshift-space distortions and the non-integrated relativistic corrections from Doppler and Sachs-Wolfe effects, thereby generalising [23] which only considered the Doppler contribution. The integrated relativistic corrections from lensing magnification and time delay effects are

¹See e.g. [9–14] for earlier work on general wide-angle correlations, without including relativistic effects.

included in the midpoint results of [22] but we omit these effects in our generalisation, leaving them for future work. We investigate the detectability of the relativistic, wide-angle and combined corrections by computing the χ^2 for two futuristic galaxy surveys and their cross power. If these corrections to the standard power spectra are detectable, then constraints on cosmological parameters could be affected when neglecting the corrections. In particular, we expect that measurements of the local primordial non-Gaussianity parameter, f_{NL} , whose signal is strongest on very large scales, could be affected by relativistic wide-angle corrections.

We consider linear scalar perturbations on a late-time flat Λ CDM background, in the Newtonian gauge. The perturbed metric is

$$ds^2 = a^2(\eta) \left[- (1 + 2\Phi) d\eta^2 + (1 - 2\Phi) d\mathbf{x}^2 \right], \quad (1.1)$$

where a is the scale factor, η is conformal time and Φ is the gravitational potential. The matter 4-velocity is

$$u^\mu = \frac{1}{a} (1 - \Phi, v^i), \quad (1.2)$$

where the peculiar velocity $v^i = dx^i/d\eta = a u^i$ is irrotational, so that $v_i = \partial_i V$, where V is the velocity potential.

2 Relativistic and wide-angle corrections in the number counts

For a given source population a , the dominant terms in the redshift-space number density contrast at linear order (see [24] for beyond-linear effects) are

$$\Delta_a(z, \mathbf{x}_a) = b_a(z) \delta(z, \mathbf{x}_a) - \frac{1}{\mathcal{H}(z)} \partial_{\parallel}^2 V(z, \mathbf{x}_a), \quad (2.1)$$

where $|\mathbf{x}_a|$ is the background comoving line-of-sight distance to the background redshift z , b_a is the bias of tracer a , $\mathcal{H} = (1+z)^{-1} H = H_0 (1+z)^{-1} [(1+z)^3 \Omega_{m0} + 1 - \Omega_{m0}]^{1/2}$ is the conformal Hubble parameter, δ is the comoving matter density contrast, and $\partial_{\parallel} = \hat{\mathbf{x}}_a \cdot \nabla$ is the derivative along the line of sight $\hat{\mathbf{x}}_a$. In Fourier space (2.1) is

$$\Delta_a(z, \mathbf{k}, \hat{\mathbf{x}}_a) = \left[b_a(z) + f(z) (\hat{\mathbf{k}} \cdot \hat{\mathbf{x}}_a)^2 \right] \delta(z, \mathbf{k}), \quad (2.2)$$

where $f = -d \ln D / d \ln(1+z)$ is the linear matter growth rate, D is the growth factor (normalized to 1 today), and we used the continuity equation $V = -(\mathcal{H}/k^2) f \delta$.

First, we consider the non-integrated relativistic corrections to the density contrast in (2.1), which are the Doppler (D) and gravitational potential (Φ) terms. In Newtonian gauge [4]:

$$\Delta_a^{\text{D}}(z, \mathbf{x}_a) = \left[\mathcal{E}_a(z) - 2 \mathcal{Q}_a(z) + \frac{2 [\mathcal{Q}_a(z) - 1]}{x_a \mathcal{H}(z)} - \frac{\mathcal{H}(z)'}{\mathcal{H}(z)^2} \right] \partial_{\parallel} V(z, \mathbf{x}_a), \quad (2.3)$$

$$\begin{aligned} \Delta_a^{\Phi}(z, \mathbf{x}_a) &= \left[-1 - \mathcal{E}_a(z) + 4 \mathcal{Q}_a(z) - \frac{2 [\mathcal{Q}_a(z) - 1]}{x_a \mathcal{H}(z)} + \frac{\mathcal{H}(z)'}{\mathcal{H}(z)^2} \right] \Phi(z, \mathbf{x}_a) \\ &+ \frac{1}{\mathcal{H}(z)} \Phi'(z, \mathbf{x}_a) + (3 - \mathcal{E}_a) \mathcal{H}(z) V(z, \mathbf{x}_a), \end{aligned} \quad (2.4)$$

where $\Phi = -(3/2)\Omega_m(\mathcal{H}/k)^2\delta$ by the Poisson equation. Here \mathcal{E} (which is often denoted b_e or f_{evo}) and \mathcal{Q} ($= 5s/2$) are the evolution and magnification biases (see e.g. [25]):

$$\mathcal{E}_a = -\frac{\partial \ln n_a}{\partial \ln(1+z)}, \quad \mathcal{Q}_a = -\frac{\partial \ln n_a}{\partial \ln L_{c,a}}, \quad (2.5)$$

where n_a is the background comoving number density of sample a and $L_{c,a}$ is the luminosity cut of the sources detected, given the specifications of the survey under consideration.

It is important to highlight the point that here δ is the matter density contrast in comoving gauge. When we include ultra-large scale effects from relativistic or wide-angle corrections, it is advisable to use the comoving density contrast δ [4, 26]. If this is not done, then two important relations above break down on ultra-large scales and need to be modified: (a) the scale-independent bias relation $\delta_a(z, \mathbf{k}) = b_a(z) \delta(z, \mathbf{k})$, and (b) the simple form of the Poisson equation, $\nabla^2 \Phi \propto \delta$.

In Fourier space, (2.3) and (2.4) may be written as

$$\Delta_a^{\text{D}} = i \frac{1}{k} \gamma_a^{\text{D}}(\hat{\mathbf{k}} \cdot \hat{\mathbf{x}}_a) \delta \quad \text{and} \quad \Delta_a^{\Phi} = \frac{1}{k^2} \gamma_a^{\Phi} \delta, \quad (2.6)$$

where

$$\gamma_a^{\text{D}} = \mathcal{H} f \left[\mathcal{E}_a - 2\mathcal{Q}_a + \frac{2(\mathcal{Q}_a - 1)}{x_a \mathcal{H}} - \frac{\mathcal{H}'}{\mathcal{H}^2} \right], \quad (2.7)$$

$$\gamma_a^{\Phi} = \frac{3}{2} \Omega_m \mathcal{H}^2 \left[2 + \mathcal{E}_a - f - 4\mathcal{Q}_a + \frac{2(\mathcal{Q}_a - 1)}{x_a \mathcal{H}} - \frac{\mathcal{H}'}{\mathcal{H}^2} \right] + \mathcal{H}^2 f(3 - \mathcal{E}_a). \quad (2.8)$$

From now on, we neglect terms in the 2-point correlations $\langle \Delta_a \Delta_b \rangle$, i.e. quadratic in the density contrast, that are of order $\delta(\mathcal{H}/k)^n$, where $n > 2$. For consistency, all terms with $n \leq 2$ should be included in the 2-point correlations and power spectra.

The relativistic corrections are added to the density contrast in (2.2) to give

$$\begin{aligned} \Delta_a(z, \mathbf{k}, \hat{\mathbf{x}}_a) &= \left[b_a(z) + f(z)(\hat{\mathbf{k}} \cdot \hat{\mathbf{x}}_a)^2 + i \frac{1}{k} \gamma_a^{\text{D}}(z)(\hat{\mathbf{k}} \cdot \hat{\mathbf{x}}_a) + \frac{1}{k^2} \gamma_a^{\Phi}(z) \right] \delta(z, \mathbf{k}) \\ &= \mathcal{K}_a(z, \mathbf{k}, \hat{\mathbf{x}}_a) \delta(z, \mathbf{k}), \end{aligned} \quad (2.9)$$

where \mathcal{K}_a is the total Fourier kernel for tracer a . Typically (2.9) is simplified using the plane-parallel approximation. However, the inclusion of relativistic corrections naturally requires the additional inclusion of wide-angle corrections, which are of the same parametric order, i.e. $O[\delta(\mathcal{H}/k)]$. In order to implement wide-angle corrections, we need to specify the geometric set-up.

We choose a line-of-sight vector \mathbf{r} from the observer to the separation vector $\mathbf{x}_{ab} = \mathbf{x}_a - \mathbf{x}_b$ (see Figure 1):

$$\mathbf{x}_a = \mathbf{r} - (1-t)\mathbf{x}_{ab} \quad \text{and} \quad \mathbf{x}_b = \mathbf{r} + t\mathbf{x}_{ab}, \quad (2.10)$$

where $0 \leq t \leq 1$. The endpoint ($t = 0$ or 1) and midpoint ($t = 1/2$) are typical choices.

Then we define the perturbation parameter vector [22]

$$\boldsymbol{\epsilon} = \frac{\mathbf{x}_{ab}}{r}, \quad (2.11)$$

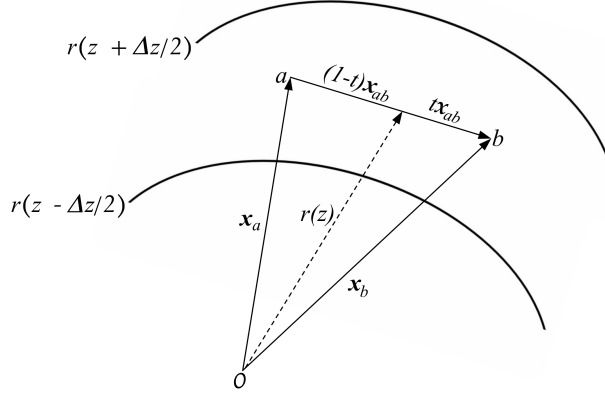


Figure 1. Geometry of the two-point correlation function for a pair of fluctuations.

which requires that the galaxy separation is less than the line-of-sight distance, i.e., $x_{ab} < r$ (see [17] for a detailed discussion of the validity of the perturbative wide-angle expansion). In Fourier space, $x_{ab} < r$ imposes a minimum $k_\epsilon(z)$ for the validity of the perturbative expansion:

$$k > k_\epsilon(z) = \frac{1}{r(z)}. \quad (2.12)$$

We follow [22] in neglecting the radial variations in a redshift bin, effectively treating all quantities in a bin as at the mid-redshift. Although it is straightforward to include these corrections (see [23]) they significantly complicate the expressions and we leave their inclusion for future work. An example of the effect of radial corrections is shown in Figure 5 below.

We rewrite (2.10) as

$$\mathbf{x}_a = [\hat{\mathbf{r}} - (1-t)\boldsymbol{\epsilon}]r \quad \text{and} \quad \mathbf{x}_b = (\hat{\mathbf{r}} + t\boldsymbol{\epsilon})r. \quad (2.13)$$

Taking the products $\mathbf{x}_a \cdot \mathbf{x}_a$, it follows that

$$\frac{1}{x_a} = \frac{1}{r} \left[1 + (1-t)(\boldsymbol{\epsilon} \cdot \hat{\mathbf{r}}) + \frac{3}{2}(1-t)^2(\boldsymbol{\epsilon} \cdot \hat{\mathbf{r}})^2 - \frac{1}{2}(1-t)^2\epsilon^2 \right], \quad (2.14)$$

$$\frac{1}{x_b} = \frac{1}{r} \left[1 - t(\boldsymbol{\epsilon} \cdot \hat{\mathbf{r}}) + \frac{3}{2}t^2(\boldsymbol{\epsilon} \cdot \hat{\mathbf{r}})^2 - \frac{1}{2}t^2\epsilon^2 \right]. \quad (2.15)$$

Here, and in the remainder of the paper, we neglect terms of $\mathcal{O}(\epsilon^3)$. Consequently, from now on all relevant expressions are implicitly understood to hold up to $\mathcal{O}(\epsilon^2, \delta(\mathcal{H}/k)^2)$. Using the above results in (2.13), we obtain

$$\hat{\mathbf{x}}_a = \left[1 + (1-t)(\boldsymbol{\epsilon} \cdot \hat{\mathbf{r}}) + \frac{3}{2}(1-t)^2(\boldsymbol{\epsilon} \cdot \hat{\mathbf{r}})^2 - \frac{1}{2}(1-t)^2\epsilon^2 \right] \hat{\mathbf{r}} - (1-t)[1 + (1-t)(\boldsymbol{\epsilon} \cdot \hat{\mathbf{r}})]\boldsymbol{\epsilon}, \quad (2.16)$$

$$\hat{\mathbf{x}}_b = \left[1 - t(\boldsymbol{\epsilon} \cdot \hat{\mathbf{r}}) + \frac{3}{2}t^2(\boldsymbol{\epsilon} \cdot \hat{\mathbf{r}})^2 - \frac{1}{2}t^2\epsilon^2 \right] \hat{\mathbf{r}} + t[1 - t(\boldsymbol{\epsilon} \cdot \hat{\mathbf{r}})]\boldsymbol{\epsilon}. \quad (2.17)$$

We decompose \mathbf{k} and $\boldsymbol{\epsilon}$ into their Cartesian components (k_x, k_y, k_z) , taking the z -axis to be along the line of sight \mathbf{r} to redshift z . Then using (2.16) and (2.17), we can write the total Fourier kernel given in (2.9) as

$$\mathcal{K}_a = \mathcal{K}_a^{\text{S}} + \mathcal{K}_a^{\text{R}} + \mathcal{K}_a^{\text{W}} + \mathcal{K}_a^{\text{RW}}, \quad (2.18)$$

where the \mathcal{K}_a^{I} are as follows.

- S: The standard Newtonian plane-parallel Kaiser part:

$$\mathcal{K}_a^S = b_a + f \left(\frac{k_z}{k} \right)^2 \quad \text{where} \quad k_z = \mathbf{k} \cdot \hat{\mathbf{r}} \equiv \mu k. \quad (2.19)$$

- R: The plane-parallel relativistic corrections to the standard kernel:

$$\mathcal{K}_a^R = \mathcal{K}_a^D + \mathcal{K}_a^\Phi, \quad \text{where} \quad \mathcal{K}_a^D = i \frac{k_z}{k} \gamma_a^D, \quad \mathcal{K}_a^\Phi = \frac{1}{k^2} \gamma_a^\Phi. \quad (2.20)$$

- W: The Newtonian wide-angle corrections to the standard kernel:

$$\mathcal{K}_a^W, \text{ given in } \text{Appendix A}.$$

- RW: The wide-angle corrections to the plane-parallel relativistic kernel:

$$\mathcal{K}_a^{\text{RW}}, \text{ given in } \text{Appendix A}.$$

Then the full kernel, i.e. standard + combined relativistic and wide-angle corrections, is

$$\mathcal{K}_a = \mathcal{K}_a^S + \mathcal{K}_a^W + \mathcal{K}_a^R + \mathcal{K}_a^{\text{RW}}. \quad (2.21)$$

3 Auto- and cross-power spectra

The Fourier power spectra are

$$P_{ab}(\mathbf{k}, \mathbf{r}) = \int \frac{d^3 \mathbf{k}'}{(2\pi)^3} \int d^3 \boldsymbol{\epsilon} r e^{-i \mathbf{r}(\mathbf{k}-\mathbf{k}') \cdot \boldsymbol{\epsilon}} \mathcal{K}_a(\mathbf{k}', \boldsymbol{\epsilon}, \mathbf{r}) \mathcal{K}_b^*(\mathbf{k}', \boldsymbol{\epsilon}, \mathbf{r}) P(k'), \quad (3.1)$$

where P is the linear power spectrum of the comoving matter density contrast δ . Here and below, we omit the dependencies on z for brevity. These are the ‘local’ power spectra, i.e. the Fourier power spectra at line-of-sight position $\mathbf{r}(z)$. The ‘full’ power spectra are then given by an integral over all lines of sight [22],

$$P_{ab}^{\text{full}}(\mathbf{k}) = \frac{1}{V_s} \int d^3 \mathbf{r} P_{ab}(\mathbf{k}, \mathbf{r}), \quad (3.2)$$

where $V_s(z)$ is the survey volume. In this paper we will work with the local power spectra.

The product of Fourier kernels in (3.1) can be written in the form [22]:

$$\mathcal{K}_a(\mathbf{k}', \boldsymbol{\epsilon}, \mathbf{r}) \mathcal{K}_b^*(\mathbf{k}', \boldsymbol{\epsilon}, \mathbf{r}) = \sum_{l,m,n} \mathcal{C}_{lmn}^{(ab)}(\mathbf{k}', \mathbf{r}) \epsilon_x^l \epsilon_y^m \epsilon_z^n \quad \text{where} \quad l + m + n \leq 2. \quad (3.3)$$

Here the coefficients $\mathcal{C}_{lmn}^{(ab)}$ are independent of $\boldsymbol{\epsilon}$ and the condition on l, m, n excludes terms of $\mathcal{O}(\epsilon^3)$. Then the power spectrum (3.1) becomes

$$P_{ab}(\mathbf{k}, \mathbf{r}) = \sum_{l,m,n} \int \frac{d^3 \mathbf{k}'}{(2\pi)^3} \int d^3 \mathbf{x}_{ab} e^{-i(\mathbf{k}-\mathbf{k}') \cdot \mathbf{x}_{ab}} \epsilon_x^l \epsilon_y^m \epsilon_z^n \mathcal{C}_{lmn}^{(ab)}(\mathbf{k}', \mathbf{r}) P(k'), \quad (3.4)$$

where $r d^3 \boldsymbol{\epsilon} = d^3 \mathbf{x}_{ab}$ from (2.11). The useful relation

$$e^{-i(\mathbf{k}-\mathbf{k}') \cdot \mathbf{x}_{ab}} \epsilon_x^l \epsilon_y^m \epsilon_z^n = \left(\frac{-i}{r} \right)^{l+m+n} \left(\frac{\partial}{\partial k'_x} \right)^l \left(\frac{\partial}{\partial k'_y} \right)^m \left(\frac{\partial}{\partial k'_z} \right)^n \left[e^{-i(\mathbf{k}-\mathbf{k}') \cdot \mathbf{x}_{ab}} \right], \quad (3.5)$$

leads to

$$P_{ab} = \sum_{l,m,n} \left(\frac{-i}{r} \right)^{l+m+n} \int \frac{d^3 \mathbf{k}'}{(2\pi)^3} I_{lmn}^{(ab)}, \quad (3.6)$$

where

$$I_{lmn}^{(ab)} = \mathcal{C}_{lmn}^{(ab)} P \left(\frac{\partial}{\partial k'_x} \right)^l \left(\frac{\partial}{\partial k'_y} \right)^m \left(\frac{\partial}{\partial k'_z} \right)^n \int d^3 \mathbf{x}_{ab} e^{-i(\mathbf{k}-\mathbf{k}') \cdot \mathbf{x}_{ab}}. \quad (3.7)$$

Here we moved the ϵ -independent coefficients and derivative operators out of the \mathbf{x}_{ab} integral, which gives the 3D Dirac-delta function:

$$\int d^3 \mathbf{x}_{ab} e^{i(\mathbf{k}'-\mathbf{k}) \cdot \mathbf{x}_{ab}} = (2\pi)^3 \delta^{\text{Dirac}}(\mathbf{k}' - \mathbf{k}). \quad (3.8)$$

Using the identity

$$\int dx f(x) \frac{\partial^q}{\partial x^q} [\delta^{\text{Dirac}}(x - x_0)] = (-1)^q \frac{\partial^q}{\partial x^q} f(x) \Big|_{x=x_0}, \quad (3.9)$$

we find that

$$\begin{aligned} P_{ab} &= \sum_{l,m,n} \left(\frac{i}{r} \right)^{l+m+n} \left(\frac{\partial}{\partial k'_x} \right)^l \left(\frac{\partial}{\partial k'_y} \right)^m \left(\frac{\partial}{\partial k'_z} \right)^n [\mathcal{C}_{lmn}^{(ab)} P] \\ &= P_{ab}^{\text{S}} + P_{ab}^{\text{R}} + P_{ab}^{\text{W}} + P_{ab}^{\text{RW}}. \end{aligned} \quad (3.10)$$

The non-vanishing coefficients $\mathcal{C}_{lmn}^{(ab)}$ in (3.10) are given in [Appendix B](#) and the individual spectra on the right of (3.10) are as follows:

$$P_{ab}^{\text{S}} = \mathcal{K}_a^{\text{S}} \mathcal{K}_b^{\text{S}} P, \quad (3.11)$$

$$P_{ab}^{\text{R}} = [\mathcal{K}_a^{\text{S}} \mathcal{K}_b^{\text{D}*} + \mathcal{K}_b^{\text{S}} \mathcal{K}_a^{\text{D}} + \mathcal{K}_a^{\text{S}} \mathcal{K}_b^{\Phi} + \mathcal{K}_b^{\text{S}} \mathcal{K}_a^{\Phi} + \mathcal{K}_a^{\text{D}} \mathcal{K}_b^{\text{D}*}] P, \quad (3.12)$$

$$\begin{aligned} P_{ab}^{\text{W}} &= \frac{1}{(kr)^2} f \left\{ 8t(1-t) f \mu^2 [1 + 2\mu^2(-5 + 6\mu^2)] \right. \\ &\quad + 2\mu^2(-7 + 10\mu^2) [t^2 k \partial_k \mathcal{K}_a^{\text{S}} + (1-t)^2 k \partial_k \mathcal{K}_b^{\text{S}}] \\ &\quad + 4\mu^3 [t^2 k \partial_{k_z} \mathcal{K}_a^{\text{S}} + (1-t)^2 k \partial_{k_z} \mathcal{K}_b^{\text{S}}] \\ &\quad + (1-\mu^2)(-1 + 4\mu^2) [t^2 k^2 \partial_k^2 \mathcal{K}_a^{\text{S}} + (1-t)^2 k^2 \partial_k^2 \mathcal{K}_b^{\text{S}}] \\ &\quad \left. + 2(1-\mu^2)\mu [t^2 k^2 \partial_{k_z} \partial_k \mathcal{K}_a^{\text{S}} + (1-t)^2 k^2 \partial_{k_z} \partial_k \mathcal{K}_b^{\text{S}}] \right\} P \\ &\quad + i \frac{2}{kr} f \mu \left\{ 2\mu^2 [t \mathcal{K}_a^{\text{S}} - (1-t) \mathcal{K}_b^{\text{S}}] \right. \\ &\quad \left. + (1-\mu^2) [t k \partial_k \mathcal{K}_a^{\text{S}} - (1-t) k \partial_k \mathcal{K}_b^{\text{S}}] \right\} P \\ &\quad + \frac{2}{(kr)^2} f \left\{ 2t(1-t) f \mu^2 (1-\mu^2)(-2 + 9\mu^2) \right. \end{aligned}$$

$$\begin{aligned}
& + \mu^2(-7 + 10\mu^2) \left[t^2 \mathcal{K}_a^S + (1-t)^2 \mathcal{K}_b^S \right] \\
& + (1 - \mu^2)(-1 + 4\mu^2) \left[t^2 k \partial_k \mathcal{K}_a^S + (1-t)^2 k \partial_k \mathcal{K}_b^S \right] \\
& + (1 - \mu^2)\mu \left[t^2 k \partial_{k_z} \mathcal{K}_a^S + (1-t)^2 k \partial_{k_z} \mathcal{K}_b^S \right] \left. \right\} k \partial_k P \\
& + i \frac{2}{kr} f \mu (1 - \mu^2) \left[t \mathcal{K}_a^S - (1-t) \mathcal{K}_b^S \right] k \partial_k P \\
& + \frac{1}{(kr)^2} f (1 - \mu^2) \left\{ 4t(1-t) f \mu^2 (1 - \mu^2) \right. \\
& \quad \left. + (-1 + 4\mu^2) \left[t^2 \mathcal{K}_a^S + (1-t)^2 \mathcal{K}_b^S \right] \right\} k^2 \partial_k^2 P, \tag{3.13}
\end{aligned}$$

$$\begin{aligned}
P_{ab}^{\text{RW}} = & f \left\{ -\frac{1}{kr} \frac{\mathcal{H}}{k} \left\{ 2\mu^2 \left[t \left(2\mathcal{Q}_b - \mathcal{E}_b + \frac{\mathcal{H}'}{\mathcal{H}^2} \right) \mathcal{K}_a^S + (1-t) \left(2\mathcal{Q}_a - \mathcal{E}_a + \frac{\mathcal{H}'}{\mathcal{H}^2} \right) \mathcal{K}_b^S \right] \right. \right. \\
& + (1 - \mu^2) \left[t \left(2\mathcal{Q}_b - \mathcal{E}_b + \frac{\mathcal{H}'}{\mathcal{H}^2} \right) k \partial_k \mathcal{K}_a^S + (1-t) \left(2\mathcal{Q}_a - \mathcal{E}_a + \frac{\mathcal{H}'}{\mathcal{H}^2} \right) k \partial_k \mathcal{K}_b^S \right] \left. \right\} \\
& + \frac{2}{(kr)^2} \left\{ (1 - 4\mu^2) \left[t(1 - \mathcal{Q}_b) \mathcal{K}_a^S + (1-t)(1 - \mathcal{Q}_a) \mathcal{K}_b^S \right] \right. \\
& \quad + (2\mu^2 - 1) \left[t(1 - \mathcal{Q}_b) k \partial_k \mathcal{K}_a^S + (1-t)(1 - \mathcal{Q}_a) k \partial_k \mathcal{K}_b^S \right] \\
& \quad \left. + \mu \left[t(1 - \mathcal{Q}_b) k \partial_{k_z} \mathcal{K}_a^S + (1-t)(1 - \mathcal{Q}_a) k \partial_{k_z} \mathcal{K}_b^S \right] \right\} \\
& + i \frac{2}{kr} \mu \left\{ 2\mu^2 \left[t \mathcal{K}_a^D - (1-t) \mathcal{K}_b^{D*} \right] \right. \\
& \quad \left. + (1 - \mu^2) \left[t k \partial_k \mathcal{K}_a^D - (1-t) k \partial_k \mathcal{K}_b^{D*} \right] \right\} \left. \right\} P \\
& + f \left\{ \frac{1}{kr} \frac{\mathcal{H}}{k} (\mu^2 - 1) \left[t \left(2\mathcal{Q}_b - \mathcal{E}_b + \frac{\mathcal{H}'}{\mathcal{H}^2} \right) \mathcal{K}_a^S + (1-t) \left(2\mathcal{Q}_a - \mathcal{E}_a + \frac{\mathcal{H}'}{\mathcal{H}^2} \right) \mathcal{K}_b^S \right] \right. \\
& \quad + \frac{2}{(kr)^2} (2\mu^2 - 1) \left[t(1 - \mathcal{Q}_b) \mathcal{K}_a^S + (1-t)(1 - \mathcal{Q}_a) \mathcal{K}_b^S \right] \\
& \quad \left. + i \frac{2}{kr} \mu (1 - \mu^2) \left[t \mathcal{K}_a^D - (1-t) \mathcal{K}_b^{D*} \right] \right\} k \partial_k P \\
& + \frac{1}{(kr)^2} f (1 - \mu^2) \left\{ 4t(1-t) f \mu^2 (1 - \mu^2) \right. \\
& \quad \left. + (4\mu^2 - 1) \left[t^2 \mathcal{K}_a^S + (1-t)^2 \mathcal{K}_b^S \right] \right\} k^2 \partial_k^2 P. \tag{3.14}
\end{aligned}$$

Note that in the expressions (3.13) and (3.14), there are real terms with a factor of $\mu \partial_{k_z} \mathcal{K}_a^S$ or $\mu \partial_{k_z} \partial_k \mathcal{K}_a^S$, which appear to be terms multiplied by an odd power of μ . However the k_z derivative introduces another factor of $\mu = k_z/k$, as can be seen in (A.5) and (A.6), so that these terms are indeed even in μ .

The multipoles of the power spectra are given by

$$P_{ab}^{I(\ell)}(k) = \frac{(2\ell + 1)}{2} \int_{-1}^{+1} d\mu P_{ab}^I(k, \mu) \mathcal{L}_\ell(\mu) \quad \text{where } I = \text{S,R,W,RW or R+W+RW.} \quad (3.15)$$

Here \mathcal{L}_ℓ are Legendre polynomials. The detailed expressions for the dominant multipoles $\ell = 0, 1, 2$ are given in [Appendix C](#).

4 Illustrating the relativistic and wide-angle effects

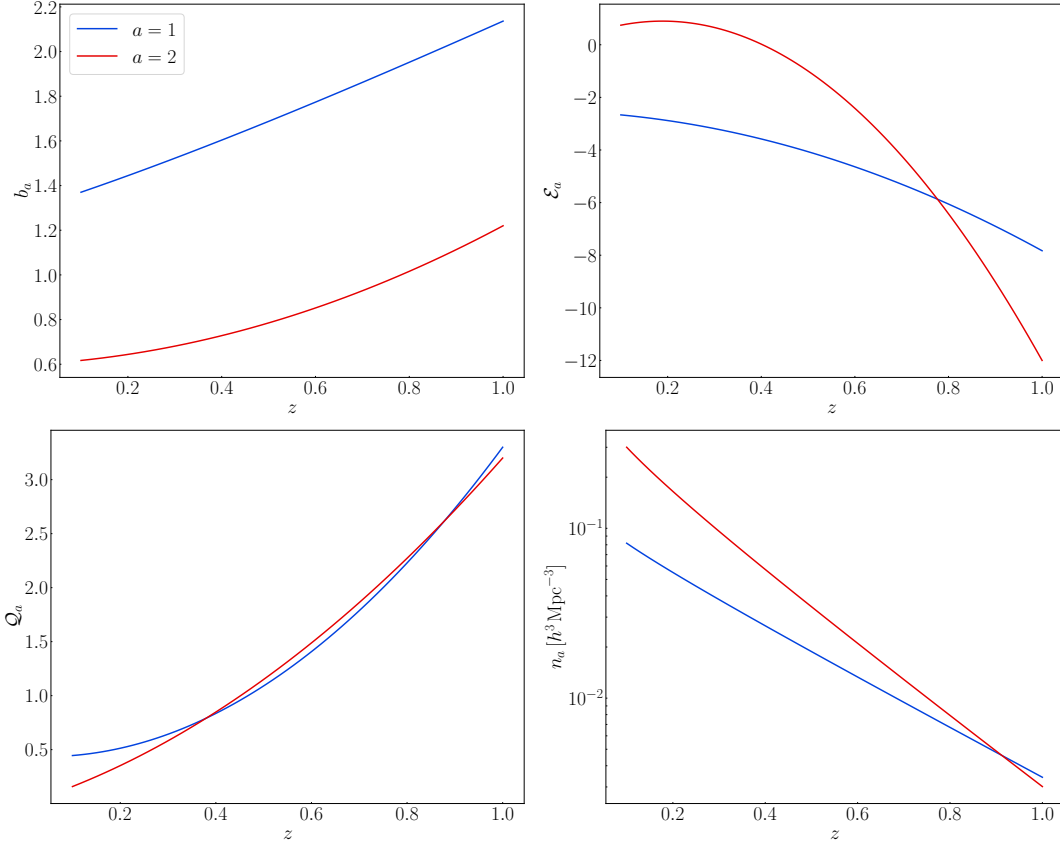


Figure 2. Clustering bias (*top left*), evolution bias (*top right*), magnification bias (*bottom left*) and number density (*bottom right*) for the 2 futuristic galaxy samples, where $a = 1$ is ‘beyond-DESI’ and $a = 2$ is SKA Phase 2.

In order to illustrate the relativistic and wide-angle effects, we need examples of galaxy samples. For each sample we require the clustering, evolution and magnification biases, together with the number densities. It is important that these quantities are *physically self-consistent*. This is achieved by using clustering biases b_a that are based on simulations or a halo model, and by deriving \mathcal{E}_a , \mathcal{Q}_a and n_a from a physically motivated luminosity function. To this end, we adapt the models described in [25] to the following futuristic mock samples:

- $a = 1$: a futuristic ‘beyond-DESI’ BGS sample with a fainter magnitude cut, $m_c = 22$.
- $a = 2$: a futuristic SKA Phase 2 HI galaxy sample with flux density cut $S_c = 5 \mu\text{Jy}$.

For the clustering biases b_a ($a = 1, 2$) we use [25]:

$$b_1 = \frac{1.3}{D(z)}, \quad b_2 = 0.60 + 0.12z + 0.50z^2. \quad (4.1)$$

We apply the futuristic flux cuts, $m_c = 22$ (for $a = 1$) and $S_c = 5 \mu\text{Jy}$ (for $a = 2$), to the luminosity function models in [25]. Then we find simple fits to the results:

$$\mathcal{E}_1 = -2.54 - 0.81z - 4.48z^2, \quad \mathcal{E}_2 = 0.2 + 7.4z - 19.6z^2, \quad (4.2)$$

$$\mathcal{Q}_1 = 0.44 - 0.26z + 3.12z^2, \quad \mathcal{Q}_2 = 1.4z + 1.8z^2, \quad (4.3)$$

$$n_1 = 0.09z^{-0.10} \exp(-3.27z) h^3 \text{Mpc}^{-3}, \quad n_2 = 0.3z^{-0.2} \exp(-4.6z) h^3 \text{Mpc}^{-3}. \quad (4.4)$$

For the redshift range and sky area, we assume

$$0.1 \leq z \leq 1, \quad \Omega_{\text{sky}} = 15\,000 \text{ deg}^2. \quad (4.5)$$

The biases b_a , \mathcal{E}_a , \mathcal{Q}_a and number densities n_a are presented in Figure 2.

Examples of the monopole and dipole of the power spectra for these galaxy samples are shown in Figure 3 and Figure 4. Note that for the midpoint line of sight, $t = 1/2$, the dipole vanishes in the auto-power case. Figure 5 presents the cross-power dipole for a different pair of tracers, i.e. 21cm intensity mapping (SKA-like) and H α galaxies (Euclid-like), at redshift $z = 1$. This further illustrates the large variety in the relativistic and wide-angle effects for different tracers. Note that the leading order relativistic contributions to the dipole do not depend on the line of sight. Furthermore, Figure 5 shows that the neglect of radial redshift derivatives can lead to non-negligible changes in signal, as shown in the (W + R) ratio for the $t = 0$ case. (See [23] for more details.)

5 Detecting the relativistic and wide-angle effects

Our aim is to test whether the detection of relativistic and wide-angle effects is feasible in futuristic galaxy surveys. Following [27], we compute the χ^2 values between the model $P_{ab}^S + P_{ab}^I$, which includes the relativistic and/or wide-angle effect I, and the standard model P_{ab}^S , which excludes the effect I. We consider all the cases of P_{ab}^I , where I=W, R, RW or W+R+RW. Our aim is to estimate the statistical significance of measuring effect I, against the null hypothesis of the absence of such an effect in the data.

In our case, we use synthetic data generated by taking the theoretical prediction of the full power spectrum (3.10). Therefore the χ^2 for effect I in a redshift bin centred at z_i is simply

$$\chi^2(z_i)^I = \sum_{k,\mu} \frac{|P_{ab}^I(z_i, k, \mu)|^2}{\text{Var}[P_{ab}(z_i, k, \mu)]}, \quad (5.1)$$

where the variance is given by

$$\text{Var}[P_{aa}] = \frac{2}{N_{\mathbf{k}}} |\tilde{P}_{aa}|^2, \quad \text{Var}[P_{12}] = \frac{1}{N_{\mathbf{k}}} \left[|\tilde{P}_{12}|^2 + |\tilde{P}_{11}| |\tilde{P}_{22}| \right]. \quad (5.2)$$

Here

$$\tilde{P}_{ab} = P_{ab} + P_{ab}^{\text{shot}} \quad \text{and} \quad P_{ab} = P_{ab}^S + P_{ab}^{\text{R+W+RW}}. \quad (5.3)$$

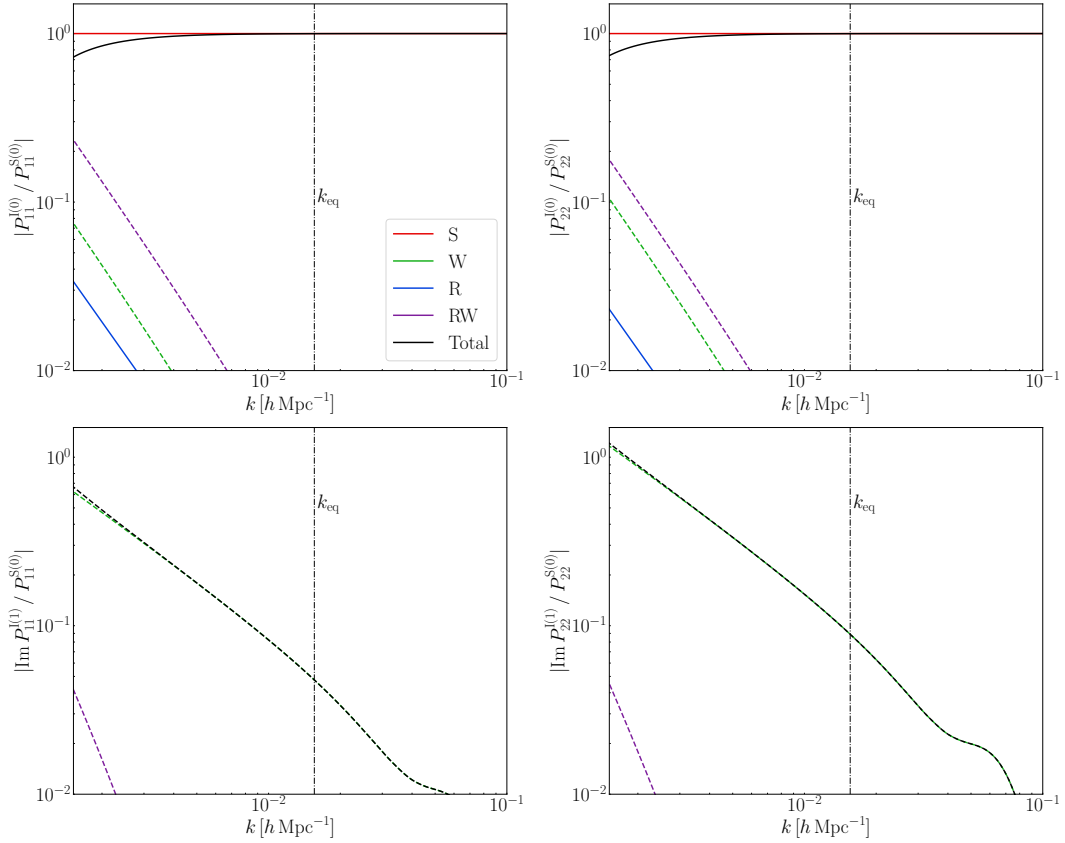


Figure 3. For the auto-power, the fractional correction to the standard monopole (*top row*) and the dipole relative to the standard monopole (*bottom row*), at $z = 0.5$. Galaxy samples are $a = 1$ (*left*) and $a = 2$ (*right*). The line of sight is endpoint, $t = 0$. Dashed lines indicate negative values.

The shot noise is given by $P_{aa}^{\text{shot}} = n_a^{-1}$ and $P_{12}^{\text{shot}} = 0$. Note that P_{ab} in the variance in (5.1)–(5.2) is given by (3.10) – i.e. it includes *all* relativistic and wide-angle effects. The number of Fourier modes in a redshift bin centred on z_i is

$$N_{\mathbf{k}}(z_i) = \frac{2\pi k^2 \Delta k \Delta \mu}{k_{\text{f}}(z_i)^3}. \quad (5.4)$$

Here the fundamental mode, $k_{\text{f}}(z_i)$, corresponds to the longest wavelength that can be measured in the redshift bin centred on z_i . The Fourier modes in each bin satisfy $k_{\text{min}}(z_i) \leq k \leq k_{\text{max}}(z_i)$, where the minimum and maximum modes are given in (5.7) and (5.8).

The χ^2 cumulative over redshift bins is

$$\chi^2(\leq z_i)^{\text{I}} = \sum_{j=1}^i \chi^2(z_j)^{\text{I}}. \quad (5.5)$$

The detection significance for effect I can be estimated as

$$\mathcal{S}(z_i)^{\text{I}} = \left[\chi^2(z_i)^{\text{I}} \right]^{1/2}, \quad (5.6)$$

and similarly for the cumulative $\mathcal{S}(\leq z_i)^{\text{I}}$.

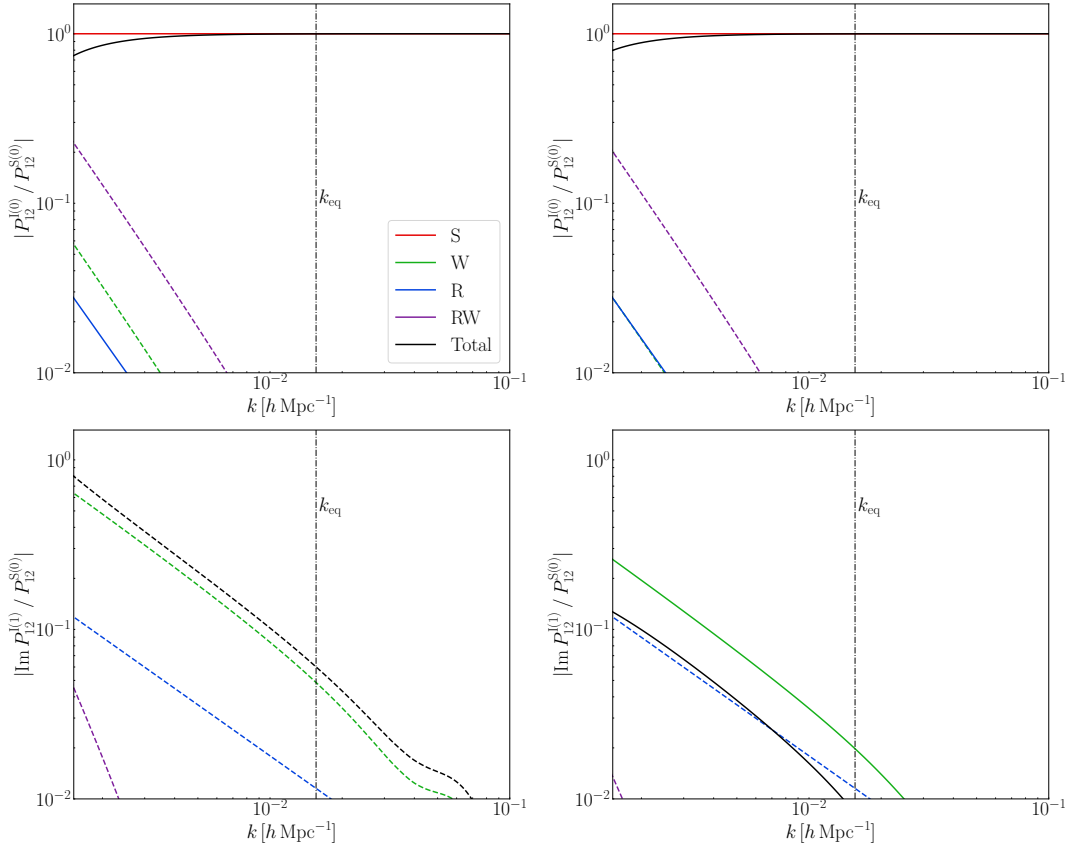


Figure 4. As in [Figure 3](#), for the cross-power between samples $a = 1$ and 2. Two configurations are shown: endpoint ($t = 0$, *left*) and midpoint ($t = 0.5$, *right*).

For the numerical calculation we choose

$$\Delta z = 0.1, \quad \Delta \mu = 0.04, \quad \Delta k = k_f, \quad k_{\max} = 0.08 (1 + z)^{2/(2+n_s)} \text{ h Mpc}^{-1}. \quad (5.7)$$

The conservative choice of k_{\max} in (5.7) means that linear perturbations remain accurate. The minimum k in each redshift bin, corresponding to the longest wavelength mode, is given by

$$k_{\min}(z) = \max [k_f(z), k_\epsilon(z)], \quad (5.8)$$

where k_ϵ is given in (2.12). These wavenumbers are shown in [Figure 6](#), confirming that $k_{\min} = k_f$ in the case of the two futuristic surveys over redshifts $z \leq 1$ and sky area $15\,000 \text{ deg}^2$.

In the cases $t = 0$ (endpoint) and $t = 0.5$ (midpoint), the results for the detection significance \mathcal{S} are summarised in [Figure 7](#) (per redshift) and [Figure 8](#) (cumulative). The significance is higher for the endpoint configuration, but in both cases, the cumulative significance is $> 5\sigma$. If we combine the signals from auto- and cross-power, the significance for the endpoint $t = 0$ line of sight is $> 10\sigma$. We note that for the midpoint line of sight, only the cross-power has a cumulative detection significance $> 5\sigma$.

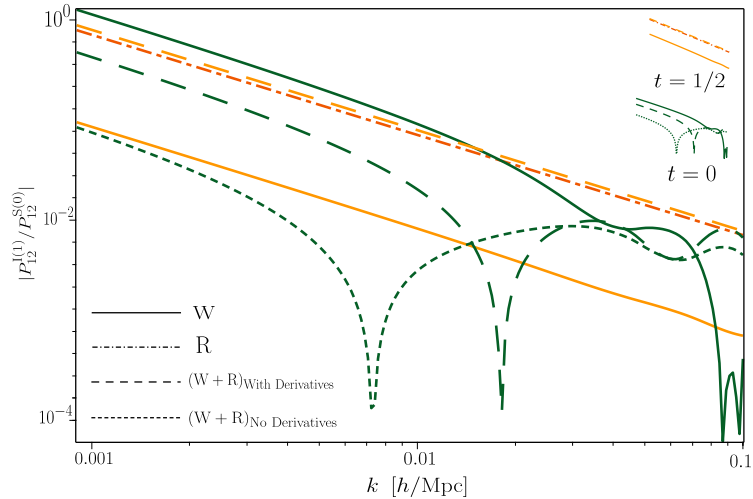


Figure 5. Imaginary part of the cross-power dipole (which is the main contributor in the imaginary part of the cross-power) as a fraction of the standard cross-power monopole. Here we use a different pair of tracers: tracer 1 is a SKA-like 21cm intensity mapping survey, while tracer 2 is a Euclid-like spectroscopic $H\alpha$ survey. The redshift is $z = 1$. The relativistic (R, red) curve is for both lines of sight, since R is independent of t . The long-dashed curves show the wide-angle + relativistic (W+R) corrections, including the radial derivative corrections, as in [23]. For $t = 0$, we show also the curves when the radial derivatives are neglected (short-dashed curve), as in the main results of this paper. To avoid clutter, we do not show the $t = 1/2$ case with no radial derivatives.

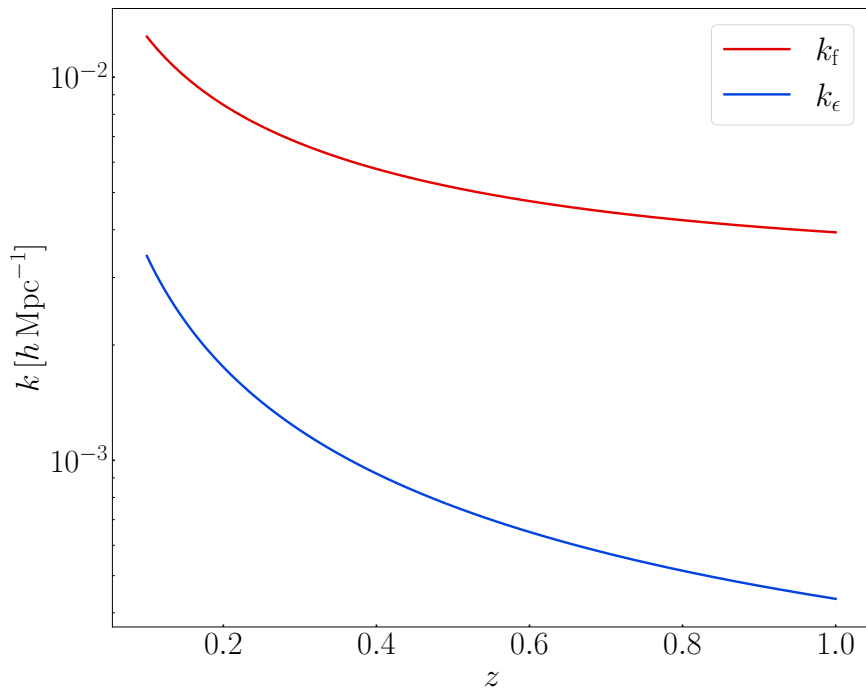


Figure 6. Longest wavelength modes in (5.8).

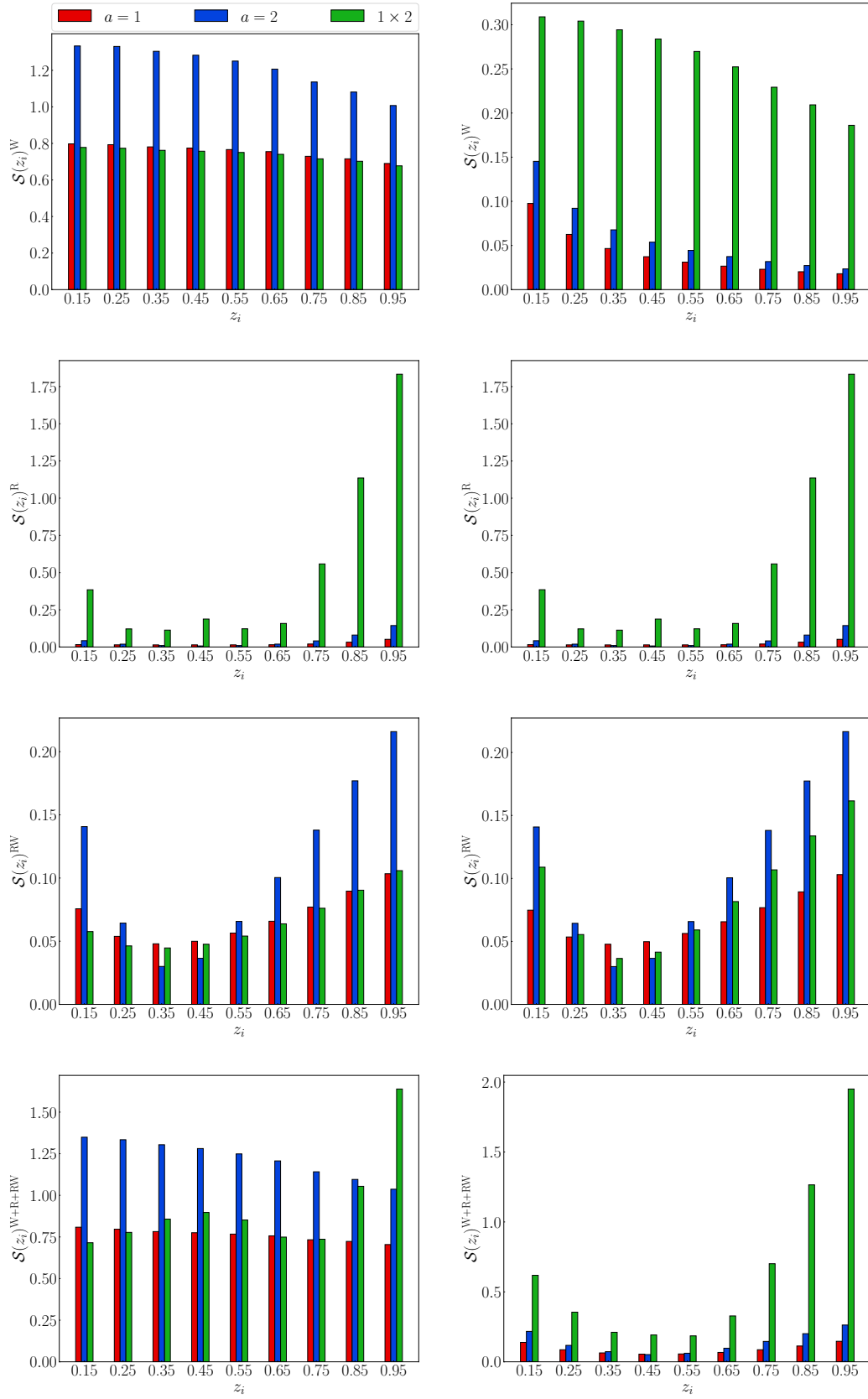


Figure 7. For the relativistic wide-angle power P_{ab}^I , where $I=R, W, RW$ or $R+W+RW$, the detection significance \mathcal{S}^I is shown in the auto- and cross-power, in each z -bin, for the endpoint ($t = 0$, left) and midpoint ($t = 0.5$, right) lines of sight.

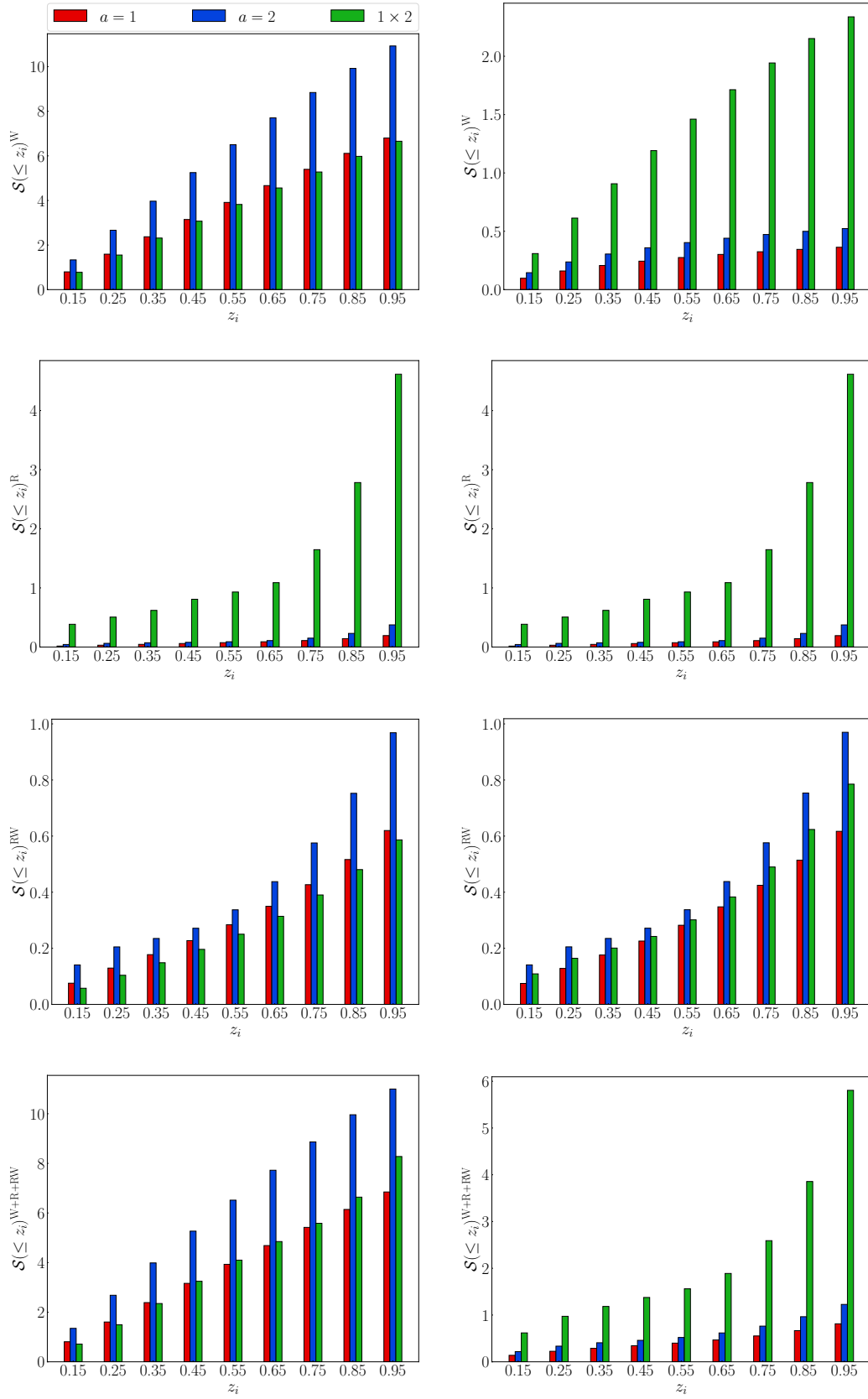


Figure 8. As in Figure 7, for the cumulative detection significance \mathcal{S} of the relativistic and wide-angle corrections in the auto- and cross-power, for the endpoint (*left*) and midpoint (*right*) lines of sight.

6 Conclusions

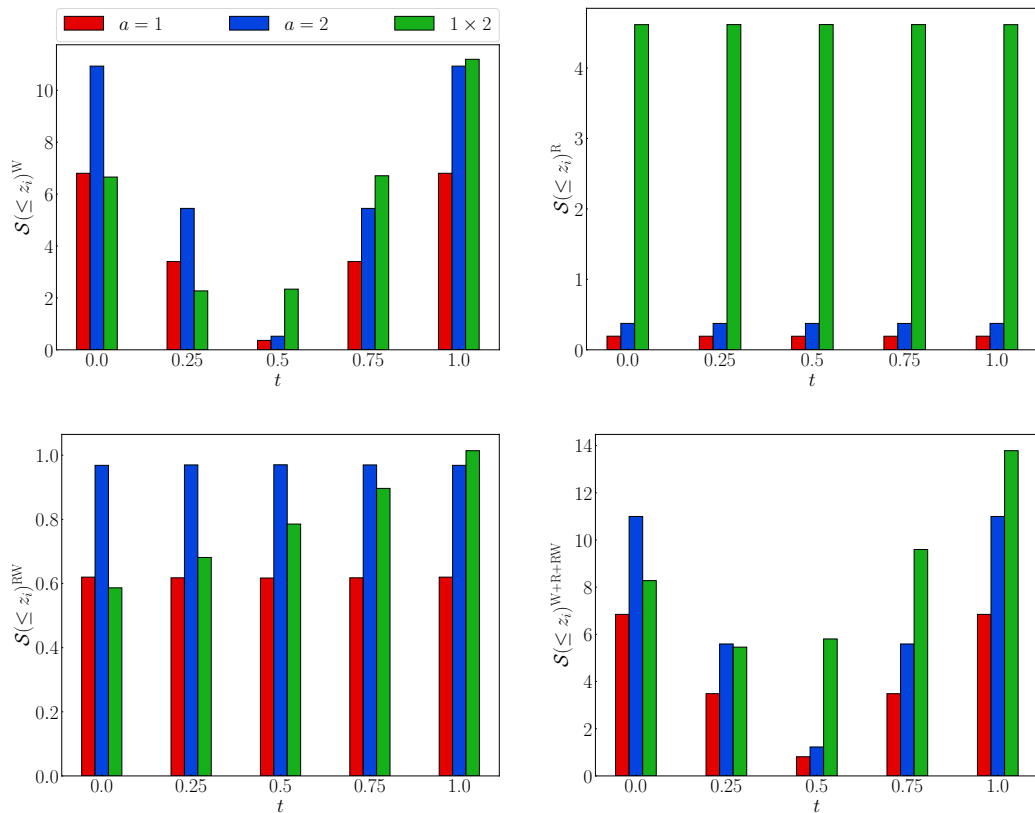


Figure 9. Cumulative detection significance \mathcal{S} of the relativistic and wide-angle corrections in the auto- and cross-power, against the line-of-sight parameter t .

This work complements the analysis presented in [22] by generalizing their power spectrum results to two tracers and to arbitrary lines of sight. We omit the integrated relativistic corrections – mainly the effect of lensing convergence – which should be reasonable at redshifts $z < 1$. The non-integrated relativistic effects in the auto-power are suppressed by a factor $O[\delta(\mathcal{H}/k)^2]$. In the imaginary part of the cross-power by contrast, there are terms $O[\delta(\mathcal{H}/k)]$ [1, 27–35]. The consequent difference in signal is clearly apparent in the \mathcal{S}^R plots in Figure 7 and Figure 8. The pure relativistic contribution is insensitive to the line-of-sight parameter t , since it is computed in the plane-parallel approximation, as in (2.20). On the other hand, the wide-angle effects are obviously sensitive to t .

Both relativistic and wide-angle effects are very sensitive to the different astrophysical properties of the surveys. Nevertheless, Figure 7 and Figure 8 show that the cumulative R+W+RW signal is detectable in the cross-power at $> 5\sigma$. For $t = 0$, the signal is also detectable in the auto-power. In this case, the combined detection significance from cross- and auto-power is $\sim 15\sigma$.

What about other values of t ? Figure 9 shows how the detection significance varies across the full range of line-of-sight parameter t . In the case of the auto-power P_{aa} , there is a symmetry about $t = 0.5$, showing that the choice of a particular line of sight t is the mirror of $1 - t$. This symmetry is broken in the case of the cross-power P_{12} , because the permutation

of the tracers leads to different power spectra, as seen in the detailed forms (3.13) and (3.14). The results for the futuristic surveys indicate significant detection potential $\sim 10\sigma$ for the cross-power P_{12} with $t = 1$, and for the auto-power P_{22} with $t = 0, 1$. The highest detection significance is in the $t = 1$ configuration, where the combined detection significance is $> 15\sigma$.

Our results show that future galaxy surveys, and even more their multi-tracer combination, should be able to detect the combined relativistic and wide-angle contributions to the power spectra, assuming that other surveys can measure the clustering, evolution and magnification biases with reasonable uncertainties – and also assuming that ultra-large scale systematics can be dealt with. This detectability is dependent on the choice of the line-of-sight parameter t , with the strongest detectability for $t = 1$ (see Figure 9). The choice of t has significant implications for computation, so it is useful that the signal is detectable in all cases we considered. Detectability means that constraints on cosmological parameters could be affected by omitting these corrections to the standard power spectra. In particular, we expect that measurements of the local primordial non-Gaussianity parameter f_{NL} could be affected by these corrections. Future work will look at Fisher forecasts on f_{NL} and other cosmological parameters [36].

Acknowledgements

SJ is supported by the Stellenbosch University Astrophysics Research Group fund. SG and RM are supported by the South African Radio Astronomy Observatory and National Research Foundation (grant no. 75415). SC acknowledges support from the Italian Ministry of University and Research, PRIN 2022 ‘EXSKALIBUR – Euclid-Cross-SKA: Likelihood Inference Building for Universe Research’, from the Italian Ministry of Foreign Affairs and International Cooperation (grant no. ZA23GR03), and from the European Union – Next Generation EU. We used the Python code Sympy for analytical calculations.

A Fourier kernels

Recall that throughout the paper we work to $\mathcal{O}[\epsilon^2, \delta(\mathcal{H}/k)^2]$.

$$\begin{aligned} \mathcal{K}_a^{\text{W}} = & \frac{f}{k^2} \left\{ (t - \sigma_a)^2 \left[(k_x^2 - k_z^2) \epsilon_x^2 + (k_y^2 - k_z^2) \epsilon_y^2 \right. \right. \\ & \left. \left. + 2(k_x k_y \epsilon_x \epsilon_y - k_x k_z \epsilon_x \epsilon_z - k_y k_z \epsilon_y \epsilon_z) \right] \right. \\ & \left. + 2(t - \sigma_a) \left[k_x k_z \epsilon_x + k_y k_z \epsilon_y \right] \right\}, \end{aligned} \quad (\text{A.1})$$

$$\begin{aligned} \mathcal{K}_a^{\text{RW}} = & i \frac{1}{k} \frac{\mathcal{H}}{k} f \left\{ \frac{2(1 - \mathcal{Q}_a)}{r\mathcal{H}} \left[(t - \sigma_a) k_z \epsilon_z \right. \right. \\ & \left. \left. + \frac{1}{2} (t - \sigma_a)^2 \left(k_z (\epsilon_x^2 + \epsilon_y^2 - 2\epsilon_z^2) + 2(k_x \epsilon_x + k_y \epsilon_y) \epsilon_z \right) \right] \right. \\ & \left. + \left[2\mathcal{Q}_a - \mathcal{E}_a + \frac{2(1 - \mathcal{Q}_a)}{r\mathcal{H}} + \frac{\mathcal{H}'}{\mathcal{H}^2} \right] \left[- (t - \sigma_a) (k_x \epsilon_x + k_y \epsilon_y) \right. \right. \\ & \left. \left. + \frac{1}{2} (t - \sigma_a)^2 \left(k_z (\epsilon_x^2 + \epsilon_y^2) + 2(k_x \epsilon_x + k_y \epsilon_y) \epsilon_z \right) \right] \right\} \\ & + \frac{3}{2} \Omega_m \frac{\mathcal{H}^2}{k^2} \frac{(1 - \mathcal{Q}_a)}{r\mathcal{H}} \left[2(t - \sigma_a) \epsilon_z + (t - \sigma_a)^2 (\epsilon_x^2 + \epsilon_y^2 - 2\epsilon_z^2) \right], \end{aligned} \quad (\text{A.2})$$

where $\sigma_a = (0, 1)$.

Derivative terms that appear in power spectrum expressions are

$$\partial_k \mathcal{K}_a^{\text{S}} = -b_{a\phi} \frac{f_{\text{NL}}}{\mathcal{M}} \frac{\partial_k \mathcal{M}}{\mathcal{M}} - \frac{2}{k} f \left(\frac{k_z}{k} \right)^2, \quad (\text{A.3})$$

$$\partial_k^2 \mathcal{K}_a^{\text{S}} = 2b_{a\phi} \frac{f_{\text{NL}}}{\mathcal{M}} \frac{(\partial_k \mathcal{M})^2}{\mathcal{M}^2} - b_{a\phi} \frac{f_{\text{NL}}}{\mathcal{M}} \frac{\partial_k^2 \mathcal{M}}{\mathcal{M}} + \frac{6}{k^2} f \left(\frac{k_z}{k} \right)^2, \quad (\text{A.4})$$

$$\partial_{k_z} \mathcal{K}_I^{\text{S}} = \frac{2}{k} f \frac{k_z}{k}, \quad (\text{A.5})$$

$$\partial_{k_z} \partial_k \mathcal{K}_a^{\text{S}} = -\frac{4}{k^2} f \frac{k_z}{k}, \quad (\text{A.6})$$

$$\partial_k \mathcal{K}_a^{\text{D}} = -\frac{2}{k} \mathcal{K}_a^{\text{D}}, \quad (\text{A.7})$$

where f_{NL} is the local primordial non-Gaussianity parameter, $b_{a\phi}$ is the primordial non-Gaussian bias and

$$\mathcal{M}(k, z) = \frac{2D(z) T(k) k^2}{3\Omega_{m0} H_0^2 g_{\text{dec}}}. \quad (\text{A.8})$$

Here D is the linear growth factor, normalised to 1 at $z = 0$, $T(k)$ is the matter transfer function, normalised to 1 at $k = 0$, and g_{dec} is the metric potential growth factor at decoupling.

B Coefficients $C_{lmn}^{(ab)}$

$$C_{000}^{(ab)} = \mathcal{K}_a^S \mathcal{K}_b^S + \mathcal{K}_a^D \mathcal{K}_b^{D*} + \mathcal{K}_a^S \mathcal{K}_b^{D*} + \mathcal{K}_b^S \mathcal{K}_a^D + \mathcal{K}_a^S \mathcal{K}_b^\Phi + \mathcal{K}_b^S \mathcal{K}_a^\Phi \quad (\text{B.1})$$

$$C_{001}^{(ab)} = \frac{1}{(kr)} \left\{ 3\Omega_m \left(\frac{\mathcal{H}}{k} \right) \left[t(1 - \mathcal{Q}_b) \mathcal{K}_a^S - (1 - t)(1 - \mathcal{Q}_a) \mathcal{K}_b^S \right] \right. \\ \left. - i 2f \frac{k_z}{k} \left[(1 - t)(1 - \mathcal{Q}_a) (\mathcal{K}_b^S + \mathcal{K}_b^{D*}) + t(1 - \mathcal{Q}_b) (\mathcal{K}_a^S + \mathcal{K}_a^D) \right] \right\} \quad (\text{B.2})$$

$$C_{010}^{(ab)} = 2f \frac{k_y}{k} \frac{k_z}{k} \left[t (\mathcal{K}_a^S + \mathcal{K}_a^D + \mathcal{K}_a^\Phi) - (1 - t) (\mathcal{K}_b^S + \mathcal{K}_b^{D*} + \mathcal{K}_b^\Phi) \right] \quad (\text{B.3})$$

$$+ i f \frac{k_y}{k} \left\{ \frac{2}{(kr)} \left[t(1 - \mathcal{Q}_b) (\mathcal{K}_a^S + \mathcal{K}_a^D) + (1 - t)(1 - \mathcal{Q}_a) (\mathcal{K}_b^S + \mathcal{K}_b^{D*}) \right] \right. \\ \left. + \left(\frac{\mathcal{H}}{k} \right) \left[(1 - t) \left(-\varepsilon_a + 2\mathcal{Q}_a + \frac{\mathcal{H}'}{\mathcal{H}^2} \right) (\mathcal{K}_b^S + \mathcal{K}_b^{D*}) \right. \right. \\ \left. \left. + t \left(-\varepsilon_b + 2\mathcal{Q}_b + \frac{\mathcal{H}'}{\mathcal{H}^2} \right) (\mathcal{K}_a^S + \mathcal{K}_a^D) \right] \right\} \quad (\text{B.4})$$

$$C_{100}^{(ab)} = C_{010}^{(ab)} \Big|_{k_y \rightarrow k_x} \quad (\text{B.5})$$

$$C_{011}^{(ab)} = -2f \frac{k_y}{k} \frac{k_z}{k} \left\{ (1 - t)^2 (\mathcal{K}_b^S + \mathcal{K}_b^{D*} + \mathcal{K}_b^\Phi) + t^2 (\mathcal{K}_a^S + \mathcal{K}_a^D + \mathcal{K}_a^\Phi) \right. \\ \left. - \frac{1}{(kr)} \left(\frac{\mathcal{H}}{k} \right) t(1 - t) \left[-3\Omega_m (2 - \mathcal{Q}_a - \mathcal{Q}_b) \right. \right. \\ \left. \left. + f \left[\left(-\varepsilon_b + 2\mathcal{Q}_b + \frac{\mathcal{H}'}{\mathcal{H}^2} \right) (1 - \mathcal{Q}_a) \right. \right. \right. \\ \left. \left. \left. + \left(-\varepsilon_a + 2\mathcal{Q}_a + \frac{\mathcal{H}'}{\mathcal{H}^2} \right) (1 - \mathcal{Q}_b) \right] \right] \right. \\ \left. - \frac{1}{(kr)^2} 4f t(1 - t)(1 - \mathcal{Q}_a)(1 - \mathcal{Q}_b) \right\} \\ + i f \frac{k_y}{k} \left\{ \frac{4}{(kr)} \left[f \left(\frac{k_z}{k} \right)^2 t(1 - t)(\mathcal{Q}_a - \mathcal{Q}_b) + (1 - t)^2 (1 - \mathcal{Q}_a) (\mathcal{K}_b^S + \mathcal{K}_b^{D*}) \right. \right. \\ \left. \left. - t^2 (1 - \mathcal{Q}_b) (\mathcal{K}_a^S + \mathcal{K}_a^D) \right] \right. \\ \left. + \left(\frac{\mathcal{H}}{k} \right) \left[(1 - t)^2 \left(-\varepsilon_a + 2\mathcal{Q}_a + \frac{\mathcal{H}'}{\mathcal{H}^2} \right) (\mathcal{K}_b^S + \mathcal{K}_b^{D*}) \right. \right. \\ \left. \left. - t^2 \left(-\varepsilon_b + 2\mathcal{Q}_b + \frac{\mathcal{H}'}{\mathcal{H}^2} \right) (\mathcal{K}_a^S + \mathcal{K}_a^D) \right] \right\} \quad (\text{B.6})$$

$$C_{101}^{(ab)} = C_{011}^{(ab)} \Big|_{k_y \rightarrow k_x} \quad (\text{B.7})$$

$$\begin{aligned}
C_{110}^{(ab)} = & 2f \frac{k_x}{k} \frac{k_y}{k} \left\{ (1-t)^2 (\mathcal{K}_b^S + \mathcal{K}_b^{D*} + \mathcal{K}_b^\Phi) + t^2 (\mathcal{K}_a^S + \mathcal{K}_a^D + \mathcal{K}_a^\Phi) \right. \\
& - f t(1-t) \left[4 \left(\frac{k_z}{k} \right)^2 + \left(\frac{\mathcal{H}}{k} \right)^2 \left[(2\mathcal{Q}_b - \mathcal{E}_b)(2\mathcal{Q}_a - \mathcal{E}_a) \right. \right. \\
& \qquad \qquad \qquad \left. \left. + \frac{\mathcal{H}'}{\mathcal{H}^2} \left(-\mathcal{E}_a - \mathcal{E}_b + 2(\mathcal{Q}_a + \mathcal{Q}_b) + \frac{\mathcal{H}'}{\mathcal{H}^2} \right) \right] \right. \\
& \qquad \qquad \qquad \left. + \frac{2}{(kr)} \left(\frac{\mathcal{H}}{k} \right) \left[\left(-\mathcal{E}_b + 2\mathcal{Q}_b + \frac{\mathcal{H}'}{\mathcal{H}^2} \right) (1 - \mathcal{Q}_a) \right. \right. \\
& \qquad \qquad \qquad \left. \left. + \left(-\mathcal{E}_a + 2\mathcal{Q}_a + \frac{\mathcal{H}'}{\mathcal{H}^2} \right) (1 - \mathcal{Q}_b) \right] \right. \\
& \qquad \qquad \qquad \left. + \frac{4}{(kr)^2} (1 - \mathcal{Q}_b)(1 - \mathcal{Q}_a) \right] \\
& \left. + i 2f \frac{k_z}{k} t(1-t) \left[\left(\frac{\mathcal{H}}{k} \right) [\mathcal{E}_b - \mathcal{E}_a - 2(\mathcal{Q}_b - \mathcal{Q}_a)] + \frac{2}{(kr)} (\mathcal{Q}_b - \mathcal{Q}_a) \right] \right\} \quad (\text{B.8})
\end{aligned}$$

$$\begin{aligned}
C_{002}^{(ab)} = & -\frac{3}{(kr)} \left(\frac{\mathcal{H}}{k} \right) \Omega_m \left[(1-t)^2 (1 - \mathcal{Q}_a) \mathcal{K}_b^S + t^2 (1 - \mathcal{Q}_b) \mathcal{K}_a^S \right] \\
& - \frac{4}{(kr)^2} f^2 \left(\frac{k_z}{k} \right)^2 t(1-t)(1 - \mathcal{Q}_a)(1 - \mathcal{Q}_b) \\
& + i \frac{2}{(kr)} f \frac{k_z}{k} \left[t^2 (1 - \mathcal{Q}_b) (\mathcal{K}_a^S + \mathcal{K}_a^D) - (1-t)^2 (1 - \mathcal{Q}_a) (\mathcal{K}_b^S + \mathcal{K}_b^{D*}) \right] \quad (\text{B.9})
\end{aligned}$$

$$\begin{aligned}
C_{020}^{(ab)} = & f \left[\left(\frac{k_y}{k} \right)^2 - \left(\frac{k_z}{k} \right)^2 \right] \left[t^2 (\mathcal{K}_a^S + \mathcal{K}_a^D + \mathcal{K}_a^\Phi) + (1-t)^2 (\mathcal{K}_b^S + \mathcal{K}_b^{D*} + \mathcal{K}_b^\Phi) \right] \\
& + \frac{1}{(kr)} \left(\frac{\mathcal{H}}{k} \right) \frac{3}{2} \Omega_m \left[t^2 (1 - \mathcal{Q}_b) \mathcal{K}_a^S + (1-t)^2 (1 - \mathcal{Q}_a) \mathcal{K}_b^S \right] \\
& - f^2 t(1-t) \left(\frac{k_y}{k} \right)^2 \left\{ 4 \left(\frac{k_z}{k} \right)^2 + \left(\frac{\mathcal{H}}{k} \right)^2 \left[(2\mathcal{Q}_b - \mathcal{E}_b)(2\mathcal{Q}_a - \mathcal{E}_a) \right. \right. \\
& \qquad \qquad \qquad \left. \left. + \frac{\mathcal{H}'}{\mathcal{H}^2} \left(-\mathcal{E}_a - \mathcal{E}_b + 2(\mathcal{Q}_a + \mathcal{Q}_b) + \frac{\mathcal{H}'}{\mathcal{H}^2} \right) \right] \right. \\
& \qquad \qquad \qquad \left. + \frac{2}{(kr)} \left(\frac{\mathcal{H}}{k} \right) \left[\left(-\mathcal{E}_b + 2\mathcal{Q}_b + \frac{\mathcal{H}'}{\mathcal{H}^2} \right) (1 - \mathcal{Q}_a) \right. \right. \\
& \qquad \qquad \qquad \left. \left. + \left(-\mathcal{E}_a + 2\mathcal{Q}_a + \frac{\mathcal{H}'}{\mathcal{H}^2} \right) (1 - \mathcal{Q}_b) \right] \right. \\
& \qquad \qquad \qquad \left. + \frac{4}{(kr)^2} (1 - \mathcal{Q}_b)(1 - \mathcal{Q}_a) \right\} \\
& + i f \left(\frac{k_z}{k} \right) \left\{ 2f \left(\frac{k_y}{k} \right)^2 t(1-t) \left[\left(\frac{\mathcal{H}}{k} \right) [\mathcal{E}_b - \mathcal{E}_a - 2(\mathcal{Q}_b - \mathcal{Q}_a)] + \frac{2}{(kr)} (\mathcal{Q}_b - \mathcal{Q}_a) \right] \right. \\
& \qquad \qquad \qquad + \frac{1}{2} \left(\frac{\mathcal{H}}{k} \right) \left[(1-t)^2 \left(-\mathcal{E}_a + 2\mathcal{Q}_a + \frac{\mathcal{H}'}{\mathcal{H}^2} \right) (\mathcal{K}_b^S + \mathcal{K}_b^{D*}) \right. \\
& \qquad \qquad \qquad \left. \left. - t^2 \left(-\mathcal{E}_b + 2\mathcal{Q}_b + \frac{\mathcal{H}'}{\mathcal{H}^2} \right) (\mathcal{K}_a^S + \mathcal{K}_a^D) \right] \right. \\
& \qquad \qquad \qquad \left. + \frac{2}{(kr)} \left[(1-t)^2 (1 - \mathcal{Q}_a) (\mathcal{K}_b^S + \mathcal{K}_b^{D*}) - t^2 (1 - \mathcal{Q}_b) (\mathcal{K}_a^S + \mathcal{K}_a^D) \right] \right\} \quad (\text{B.10})
\end{aligned}$$

$$C_{200}^{(ab)} = C_{020}^{(ab)} \Big|_{k_y \rightarrow k_x} \quad (\text{B.11})$$

C Multipoles of the power spectra

The monopoles ($\ell = 0$) for the standard, relativistic, wide-angle and cross-terms from wide-angle and relativistic contributions are

$$P_{ab}^{\text{S}(0)} = \left[\hat{b}_a \hat{b}_b + \frac{f}{3} (\hat{b}_a + \hat{b}_b) + \frac{f^2}{5} \right] P, \quad (\text{C.1})$$

$$P_{ab}^{\text{R}(0)} = \left[\frac{1}{3} \frac{1}{k^2} \gamma_a^{\text{D}} \gamma_b^{\text{D}} + \left(\frac{f}{3} + \hat{b}_b \right) \frac{1}{k^2} \gamma_a^{\Phi} + \left(\frac{f}{3} + \hat{b}_a \right) \frac{1}{k^2} \gamma_b^{\Phi} \right] P, \quad (\text{C.2})$$

$$\begin{aligned} P_{ab}^{\text{W}(0)} = & \frac{2}{105} \frac{f}{(kr)^2} \left\{ f[1 + 18t(1-t)] - 21[(1-t)^2 \hat{b}_b + t^2 \hat{b}_a] \right. \\ & - 35[(1-t)^2 k \partial_k \hat{b}_b + t^2 k \partial_k \hat{b}_a] \\ & \left. - 7[(1-t)^2 k^2 \partial_k^2 \hat{b}_b + t^2 k^2 \partial_k^2 \hat{b}_a] \right\} P \\ & + \left\{ f[11 + 30t(1-t)] - 35[(1-t)^2 \hat{b}_b + t^2 \hat{b}_a] \right. \\ & \left. - 14[(1-t)^2 k \partial_k \hat{b}_b + t^2 k \partial_k \hat{b}_a] \right\} k \partial_k P \\ & + \left\{ f[5 + 6t(1-t)] - 7[(1-t)^2 \hat{b}_b + t^2 \hat{b}_a] \right\} k^2 \partial_k^2 P \Big\}, \quad (\text{C.3}) \end{aligned}$$

$$\begin{aligned} P_{ab}^{\text{RW}(0)}(k) = & \frac{2}{15} f \left\{ - \frac{2}{kr} \left[(1-t) \frac{1}{k} \gamma_b^{\text{D}} + t \frac{1}{k} \gamma_a^{\text{D}} \right] \right. \\ & + \frac{1}{kr} \frac{\mathcal{H}}{k} \left[(1-t)(f + 5\hat{b}_b) \left(\mathcal{E}_a - 2\mathcal{Q}_a - \frac{\mathcal{H}'}{\mathcal{H}^2} \right) \right. \\ & \left. \left. + t(f + 5\hat{b}_a) \left(\mathcal{E}_b - 2\mathcal{Q}_b - \frac{\mathcal{H}'}{\mathcal{H}^2} \right) \right] \right. \\ & + \frac{5}{kr} \frac{\mathcal{H}}{k} \left[(1-t) \left(\mathcal{E}_a - 2\mathcal{Q}_a - \frac{\mathcal{H}'}{\mathcal{H}^2} \right) k \partial_k \hat{b}_b \right. \\ & \left. \left. + t \left(\mathcal{E}_b - 2\mathcal{Q}_b - \frac{\mathcal{H}'}{\mathcal{H}^2} \right) k \partial_k \hat{b}_a \right] \right. \\ & + \frac{1}{(kr)^2} \left[(1-t)(1 - \mathcal{Q}_a)(f - 5\hat{b}_b) + t(1 - \mathcal{Q}_b)(f - 5\hat{b}_a) \right] \\ & \left. - \frac{5}{(kr)^2} \left[(1-t)(1 - \mathcal{Q}_a) k \partial_k \hat{b}_b + t(1 - \mathcal{Q}_b) k \partial_k \hat{b}_a \right] \right\} P \\ & + \frac{2}{15} f \left\{ - \frac{2}{kr} \left[(1-t) \frac{1}{k} \gamma_b^{\text{D}} + t \frac{1}{k} \gamma_a^{\text{D}} \right] \right. \\ & \left. + \frac{1}{kr} \frac{\mathcal{H}}{k} \left[(1-t)(f + 5\hat{b}_b) \left(\mathcal{E}_a - 2\mathcal{Q}_a - \frac{\mathcal{H}'}{\mathcal{H}^2} \right) \right] \right\} \end{aligned}$$

$$\begin{aligned}
& + t(f + 5\hat{b}_a) \left(\mathcal{E}_b - 2\mathcal{Q}_b - \frac{\mathcal{H}'}{\mathcal{H}^2} \right) \Big] \\
& + \frac{1}{(kr)^2} \left[(1-t)(1-\mathcal{Q}_a)(f - 5\hat{b}_b) + t(1-\mathcal{Q}_b)(f - 5\hat{b}_a) \right] \Big\} k \partial_k P \\
& + \frac{1}{15} \frac{f}{(kr)^2} \left\{ -2 \left[(1-t)^2 \frac{1}{k^2} \gamma_b^\Phi + t^2 \frac{1}{k^2} \gamma_a^\Phi \right] \right. \\
& \quad + 3 \frac{\mathcal{H}}{k} \left[(1-t)^2 \left(\mathcal{E}_a - 2\mathcal{Q}_a - \frac{\mathcal{H}'}{\mathcal{H}^2} \right) \frac{1}{k} \gamma_b^D \right. \\
& \quad \quad \left. \left. + t^2 \left(\mathcal{E}_b - 2\mathcal{Q}_b - \frac{\mathcal{H}'}{\mathcal{H}^2} \right) \frac{1}{k} \gamma_a^D \right] \right. \\
& \quad \left. + 8(1-t)t \frac{\mathcal{H}^2}{k^2} f \left(\mathcal{E}_b - 2\mathcal{Q}_b - \frac{\mathcal{H}'}{\mathcal{H}^2} \right) \left(\mathcal{E}_a - 2\mathcal{Q}_a - \frac{\mathcal{H}'}{\mathcal{H}^2} \right) \right\} k^2 \partial_k^2 P, \tag{C.4}
\end{aligned}$$

where

$$\hat{b}_a = b_a + f_{\text{NL}} \frac{b_{a\phi}}{\mathcal{M}}. \tag{C.5}$$

The dipoles ($\ell = 1$) for each contribution are

$$P_{ab}^{\text{S}(1)} = 0, \tag{C.6}$$

$$P_{ab}^{\text{R}(1)} = i \frac{1}{5} \left[(3f + 5\hat{b}_b) \frac{1}{k} \gamma_a^D - (3f + 5\hat{b}_a) \frac{1}{k} \gamma_b^D \right] P, \tag{C.7}$$

$$\begin{aligned}
P_{ab}^{\text{W}(1)} = & -i \frac{4}{35} \frac{f}{kr} \left\{ \left[9(1-2t)f + 21 \left[(1-t)\hat{b}_b - t\hat{b}_a \right] \right. \right. \\
& \quad \left. \left. + 7 \left[(1-t)k \partial_k \hat{b}_b - tk \partial_k \hat{b}_a \right] \right] P \right. \\
& \quad \left. + \left[3(1-2t)f + 7 \left[(1-t)\hat{b}_b - t\hat{b}_a \right] \right] k \partial_k P \right\}, \tag{C.8}
\end{aligned}$$

$$\begin{aligned}
P_{ab}^{\text{RW}(1)} = & i \frac{1}{5} \frac{1}{(kr)^2} \frac{\mathcal{H}}{k} \left\{ -15\Omega_m \left[(1-t)(1-\mathcal{Q}_a)k \partial_k \hat{b}_b - t(1-\mathcal{Q}_b)k \partial_k \hat{b}_a \right] \right. \\
& \quad + 3f \left[(1-t)^2 \left(\mathcal{E}_a - 2\mathcal{Q}_a - \frac{\mathcal{H}'}{\mathcal{H}^2} \right) k^2 \partial_k^2 \hat{b}_b \right. \\
& \quad \quad \left. \left. - t^2 \left(\mathcal{E}_b - 2\mathcal{Q}_b - \frac{\mathcal{H}'}{\mathcal{H}^2} \right) k^2 \partial_k^2 \hat{b}_a \right] \right\} P \\
& + i \frac{1}{5} \left\{ -4 \frac{f}{kr} \left[(1-t) \frac{1}{k^2} \gamma_b^\Phi - t \frac{1}{k^2} \gamma_a^\Phi \right] \right. \\
& \quad \left. - 2 \frac{f}{kr} \frac{\mathcal{H}}{k} \left[(1-t) \left(\mathcal{E}_a - 2\mathcal{Q}_a - \frac{\mathcal{H}'}{\mathcal{H}^2} \right) \frac{1}{k} \gamma_b^D - t \left(\mathcal{E}_b - 2\mathcal{Q}_b - \frac{\mathcal{H}'}{\mathcal{H}^2} \right) \frac{1}{k} \gamma_a^D \right] \right\}
\end{aligned}$$

$$\begin{aligned}
& + \frac{2}{7} \frac{f}{(kr)^2} \frac{\mathcal{H}}{k} \left[(1-t)(21t+5)f \left(\mathcal{E}_a - 2\mathcal{Q}_a - \frac{\mathcal{H}'}{\mathcal{H}^2} \right) \right. \\
& \quad \left. + t(21t-26)f \left(\mathcal{E}_b - 2\mathcal{Q}_b - \frac{\mathcal{H}'}{\mathcal{H}^2} \right) \right. \\
& + 21(1-t)^2 \left(\mathcal{E}_a - 2\mathcal{Q}_a - \frac{\mathcal{H}'}{\mathcal{H}^2} \right) k \partial_k \hat{b}_b - 21t^2 \left(\mathcal{E}_b - 2\mathcal{Q}_b - \frac{\mathcal{H}'}{\mathcal{H}^2} \right) k \partial_k \hat{b}_a \left. \right] \\
& - \frac{6}{7} \frac{f}{(kr)^2} \left[- (1-t)^2 \frac{1}{k} \gamma_b^D + t^2 \frac{1}{k} \gamma_a^D \right] \\
& - \frac{3}{(kr)^2} \frac{\mathcal{H}}{k} \Omega_m \left[(1-t)(1-\mathcal{Q}_a)(3f+5\hat{b}_b) - t(1-\mathcal{Q}_b)(3f+5\hat{b}_a) \right] \\
& - 2 \frac{f}{(kr)^2} \left[(1-t)(1-\mathcal{Q}_a) \frac{1}{k} \gamma_b^D - t(1-\mathcal{Q}_b) \frac{1}{k} \gamma_a^D \right] \left. \right\} k \partial_k P \\
& + i \frac{1}{35} \frac{f}{(kr)^2} \left\{ \frac{\mathcal{H}}{k} \left[(1-t)(7t+9)f \left(\mathcal{E}_a - 2\mathcal{Q}_a - \frac{\mathcal{H}'}{\mathcal{H}^2} \right) + t(7t-16)f \left(\mathcal{E}_b - 2\mathcal{Q}_b - \frac{\mathcal{H}'}{\mathcal{H}^2} \right) \right. \right. \\
& \quad \left. \left. + 21(1-t)^2 \left(\mathcal{E}_a - 2\mathcal{Q}_a - \frac{\mathcal{H}'}{\mathcal{H}^2} \right) \hat{b}_b - 21t^2 \left(\mathcal{E}_b - 2\mathcal{Q}_b - \frac{\mathcal{H}'}{\mathcal{H}^2} \right) \hat{b}_a \right] \right. \\
& \quad \left. - 10 \left[(1-t)^2 \frac{1}{k} \gamma_b^D - t^2 \frac{1}{k} \gamma_a^D \right] \right\} k^2 \partial_k^2 P . \tag{C.9}
\end{aligned}$$

The quadrupoles ($\ell = 2$) are

$$P_{ab}^{S(2)} = \frac{2}{21} f \left[6f + 7\hat{b}_a + 7\hat{b}_b \right] P , \tag{C.10}$$

$$P_{ab}^{R(2)} = \frac{2}{3} \left[\frac{1}{k^2} \gamma_a^D \gamma_b^D + f \frac{1}{k^2} \gamma_a^\Phi + f \frac{1}{k^2} \gamma_b^\Phi \right] P , \tag{C.11}$$

$$\begin{aligned}
P_{ab}^{W(2)} = \frac{2}{21} \frac{f}{(kr)^2} \left\{ \right. & \left. \left\{ 2f[-13 + 54t(1-t)] - 66 \left[(1-t)^2 \hat{b}_b + t^2 \hat{b}_a \right] \right. \right. \\
& + 22 \left[(1-t)^2 k \partial_k \hat{b}_b + t^2 k \partial_k \hat{b}_a \right] \\
& \left. \left. + 11 \left[(1-t)^2 k^2 \partial_k^2 \hat{b}_b + t^2 k^2 \partial_k^2 \hat{b}_a \right] \right\} P \right. \\
& + 2 \left\{ 11 \left[(1-t)^2 k \partial_k \hat{b}_b + t^2 k \partial_k \hat{b}_a \right] + 2f[2 + 3t(1-t)] \right. \\
& \left. \left. + 11 \left[(1-t)^2 \hat{b}_b + t^2 \hat{b}_a \right] \right\} k \partial_k P \tag{C.12}
\end{aligned}$$

$$+ \left\{ 3f[1 - 2t(1-t)] + 11 \left[(1-t)^2 \hat{b}_b + t^2 \hat{b}_a \right] \right\} k^2 \partial_k^2 P \left. \right\} , \tag{C.13}$$

$$\begin{aligned}
P_{ab}^{RW(2)}(k) = \frac{2}{21} f \left\{ \right. & \left. \frac{2}{kr} \frac{\mathcal{H}}{k} \left[(1-t)(5f + 7\hat{b}_b) \left(\mathcal{E}_a - 2\mathcal{Q}_a - \frac{\mathcal{H}'}{\mathcal{H}^2} \right) \right. \right. \\
& \left. \left. + t(5f + 7\hat{b}_a) \left(\mathcal{E}_b - 2\mathcal{Q}_b - \frac{\mathcal{H}'}{\mathcal{H}^2} \right) \right] \right. \\
& \left. - \frac{7}{kr} \frac{\mathcal{H}}{k} \left[(1-t) \left(\mathcal{E}_a - 2\mathcal{Q}_a - \frac{\mathcal{H}'}{\mathcal{H}^2} \right) k \partial_k \hat{b}_b \right. \right.
\end{aligned}$$

$$\begin{aligned}
& + t \left(\mathcal{E}_b - 2\mathcal{Q}_b - \frac{\mathcal{H}'}{\mathcal{H}^2} \right) k \partial_k \hat{b}_a \Big] \\
& - \frac{20}{kr} \left[(1-t) \frac{1}{k} \gamma_b^D + t \frac{1}{k} \gamma_a^D \right] \\
& + \frac{28}{(kr)^2} \left[(1-t)(1-\mathcal{Q}_a) k \partial_k \hat{b}_b + t(1-\mathcal{Q}_b) k \partial_k \hat{b}_a \right] \\
& - \frac{2}{(kr)^2} \left[(1-t)(1-\mathcal{Q}_a)(13f + 28\hat{b}_b) \right. \\
& \quad \left. + t(1-\mathcal{Q}_b)(13f + 28\hat{b}_a) \right] \Big\} P \\
& + \frac{2}{21} f \left\{ \frac{1}{kr} \frac{\mathcal{H}}{k} \left[(1-t)(f - 7\hat{b}_b) \left(\mathcal{E}_a - 2\mathcal{Q}_a - \frac{\mathcal{H}'}{\mathcal{H}^2} \right) \right. \right. \\
& \quad \left. \left. + t(f - 7\hat{b}_a) \left(\mathcal{E}_b - 2\mathcal{Q}_b - \frac{\mathcal{H}'}{\mathcal{H}^2} \right) \right] \right. \\
& \quad - \frac{2}{kr} \left[(1-t) \frac{1}{k} \gamma_b^D + t \frac{1}{k} \gamma_a^D \right] \\
& \quad \left. + \frac{2}{(kr)^2} \left[(1-t)(1-\mathcal{Q}_a)(5f + 14\hat{b}_b) \right. \right. \\
& \quad \left. \left. + t(1-\mathcal{Q}_b)(5f + 14\hat{b}_a) \right] \right\} k \partial_k P \\
& + \frac{1}{21} \frac{f}{(kr)^2} \left\{ -16(1-t)t \frac{\mathcal{H}^2}{k^2} f \left(\mathcal{E}_a - 2\mathcal{Q}_a - \frac{\mathcal{H}'}{\mathcal{H}^2} \right) \left(\mathcal{E}_b - 2\mathcal{Q}_b - \frac{\mathcal{H}'}{\mathcal{H}^2} \right) \right. \\
& \quad + 3 \frac{\mathcal{H}}{k} \left[(1-t)^2 \left(\mathcal{E}_a - 2\mathcal{Q}_a - \frac{\mathcal{H}'}{\mathcal{H}^2} \right) \frac{1}{k} \gamma_b^D \right. \\
& \quad \left. \left. + t^2 \left(\mathcal{E}_b - 2\mathcal{Q}_b - \frac{\mathcal{H}'}{\mathcal{H}^2} \right) \frac{1}{k} \gamma_a^D \right] \right. \\
& \quad \left. + 22 \left[(1-t)^2 \frac{1}{k^2} \gamma_b^\Phi + t^2 \frac{1}{k^2} \gamma_a^\Phi \right] \right\} k^2 \partial_k^2 P . \tag{C.14}
\end{aligned}$$

References

- [1] P. McDonald, *Gravitational redshift and other redshift-space distortions of the imaginary part of the power spectrum*, *JCAP* **0911** (2009) 026, [[arXiv:0907.5220](#)].
- [2] J. Yoo, *General Relativistic Description of the Observed Galaxy Power Spectrum: Do We Understand What We Measure?*, *Phys. Rev.* **D82** (2010) 083508, [[arXiv:1009.3021](#)].
- [3] C. Bonvin and R. Durrer, *What galaxy surveys really measure*, *Phys. Rev.* **D84** (2011) 063505, [[arXiv:1105.5280](#)].
- [4] A. Challinor and A. Lewis, *The linear power spectrum of observed source number counts*, *Phys. Rev.* **D84** (2011) 043516, [[arXiv:1105.5292](#)].
- [5] D. Bertacca, R. Maartens, A. Raccanelli, and C. Clarkson, *Beyond the plane-parallel and Newtonian approach: Wide-angle redshift distortions and convergence in general relativity*, *JCAP* **1210** (2012) 025, [[arXiv:1205.5221](#)].
- [6] J. Yoo and U. Seljak, *Wide Angle Effects in Future Galaxy Surveys*, *Mon. Not. Roy. Astron. Soc.* **447** (2015), no. 2 1789–1805, [[arXiv:1308.1093](#)].
- [7] V. Tansella, G. Jelic-Cizmek, C. Bonvin, and R. Durrer, *COFFE: a code for the full-sky relativistic galaxy correlation function*, *JCAP* **10** (2018) 032, [[arXiv:1806.11090](#)].
- [8] H. S. G. Gebhardt and O. Doré, *Fabulous code for spherical Fourier-Bessel decomposition*, *Phys. Rev. D* **104** (2021), no. 12 123548, [[arXiv:2102.10079](#)].
- [9] A. S. Szalay, T. Matsubara, and S. D. Landy, *Redshift space distortions of the correlation function in wide angle galaxy surveys*, *Astrophys. J. Lett.* **498** (1998) L1, [[astro-ph/9712007](#)].
- [10] S. Bharadwaj, *Radial Redshift Space Distortions*, *Astrophys. J.* **516** (1999) 507–518, [[astro-ph/9812274](#)].
- [11] T. Matsubara, *The Correlation function in redshift space: General formula with wide angle effects and cosmological distortions*, *Astrophys. J.* **535** (2000) 1, [[astro-ph/9908056](#)].
- [12] I. Szapudi, *Wide angle redshift distortions revisited*, *Astrophys. J.* **614** (2004) 51–55, [[astro-ph/0404477](#)].
- [13] P. Papai and I. Szapudi, *Non-Perturbative Effects of Geometry in Wide-Angle Redshift Distortions*, *Mon. Not. Roy. Astron. Soc.* **389** (2008) 292, [[arXiv:0802.2940](#)].
- [14] A. Raccanelli, L. Samushia, and W. J. Percival, *Simulating Redshift-Space Distortions for Galaxy Pairs with Wide Angular Separation*, *Mon. Not. Roy. Astron. Soc.* **409** (2010) 1525, [[arXiv:1006.1652](#)].
- [15] P. H. F. Reimberg, F. Bernardeau, and C. Pitrou, *Redshift-space distortions with wide angular separations*, *JCAP* **1601** (2016), no. 01 048, [[arXiv:1506.06596](#)].
- [16] E. Castorina and M. White, *Beyond the plane-parallel approximation for redshift surveys*, *Mon. Not. Roy. Astron. Soc.* **476** (2018), no. 4 4403–4417, [[arXiv:1709.09730](#)].
- [17] J. N. Benabou, I. Sands, H. S. G. Gebhardt, C. Heinrich, and O. Doré, *Wide-Angle Effects in the Power Spectrum Multipoles in Next-Generation Redshift Surveys*, [[arXiv:2404.04811](#)].
- [18] N. Grimm, F. Scaccabarozzi, J. Yoo, S. G. Biern, and J.-O. Gong, *Galaxy Power Spectrum in General Relativity*, *JCAP* **11** (2020) 064, [[arXiv:2005.06484](#)].
- [19] F. Beutler, E. Castorina, and P. Zhang, *Interpreting measurements of the anisotropic galaxy power spectrum*, *JCAP* **03** (2019) 040, [[arXiv:1810.05051](#)].
- [20] E. Castorina and E. di Dio, *The observed galaxy power spectrum in General Relativity*, *JCAP* **01** (2022), no. 01 061, [[arXiv:2106.08857](#)].

- [21] M. Y. Elkhachab, C. Porciani, and D. Bertacca, *The large-scale monopole of the power spectrum in a Euclid-like survey: wide-angle effects, lensing, and the ‘finger of the observer’*, *Mon. Not. Roy. Astron. Soc.* **509** (2021), no. 2 1626–1645, [[arXiv:2108.13424](#)].
- [22] M. Noorikuhani and R. Scoccimarro, *Wide-angle and relativistic effects in Fourier-space clustering statistics*, *Phys. Rev. D* **107** (2023), no. 8 083528, [[arXiv:2207.12383](#)].
- [23] P. Paul, C. Clarkson, and R. Maartens, *Wide-angle effects in multi-tracer power spectra with Doppler corrections*, *JCAP* **04** (2023) 067, [[arXiv:2208.04819](#)].
- [24] S. Saga, A. Taruya, M.-A. Breton, and Y. Rasera, *Detectability of the gravitational redshift effect from the asymmetric galaxy clustering*, *Mon. Not. Roy. Astron. Soc.* **511** (2022), no. 2 2732–2754, [[arXiv:2109.06012](#)].
- [25] R. Maartens, J. Fonseca, S. Camera, S. Jolicoeur, J.-A. Viljoen, and C. Clarkson, *Magnification and evolution biases in large-scale structure surveys*, *JCAP* **12** (2021), no. 12 009, [[arXiv:2107.13401](#)].
- [26] M. Bruni, R. Crittenden, K. Koyama, R. Maartens, C. Pitrou, and D. Wands, *Disentangling non-Gaussianity, bias and GR effects in the galaxy distribution*, *Phys. Rev. D* **85** (2012) 041301, [[arXiv:1106.3999](#)].
- [27] F. Montano and S. Camera, *Detecting Relativistic Doppler in Galaxy Clustering with Tailored Galaxy Samples*, [arXiv:2309.12400](#).
- [28] C. Bonvin, L. Hui, and E. Gaztanaga, *Asymmetric galaxy correlation functions*, *Phys. Rev. D* **89** (2014), no. 8 083535, [[arXiv:1309.1321](#)].
- [29] C. Bonvin, L. Hui, and E. Gaztanaga, *Optimising the measurement of relativistic distortions in large-scale structure*, *JCAP* **1608** (2016), no. 08 021, [[arXiv:1512.03566](#)].
- [30] E. Gaztanaga, C. Bonvin, and L. Hui, *Measurement of the dipole in the cross-correlation function of galaxies*, *JCAP* **1701** (2017), no. 01 032, [[arXiv:1512.03918](#)].
- [31] V. Irsic, E. Di Dio, and M. Viel, *Relativistic effects in Lyman- α forest*, *JCAP* **1602** (2016), no. 02 051, [[arXiv:1510.03436](#)].
- [32] A. Hall and C. Bonvin, *Measuring cosmic velocities with 21 cm intensity mapping and galaxy redshift survey cross-correlation dipoles*, *Phys. Rev. D* **95** (2017), no. 4 043530, [[arXiv:1609.09252](#)].
- [33] F. Lepori, E. Di Dio, E. Villa, and M. Viel, *Optimal galaxy survey for detecting the dipole in the cross-correlation with 21 cm Intensity Mapping*, *JCAP* **1805** (2018), no. 05 043, [[arXiv:1709.03523](#)].
- [34] C. Bonvin and P. Fleury, *Testing the equivalence principle on cosmological scales*, *JCAP* **1805** (2018), no. 05 061, [[arXiv:1803.02771](#)].
- [35] F. Lepori, V. Iršič, E. Di Dio, and M. Viel, *The impact of relativistic effects on the 3D Quasar-Lyman- α cross-correlation*, *JCAP* **04** (2020) 006, [[arXiv:1910.06305](#)].
- [36] S. Guedeounme, S. Jolicoeur, and R. Maartens, *In preparation*, [arXiv:240n.nnnnn](#).